

Adversarial Reprogramming Revisited

Matthias Englert*
University of Warwick

m.englert@warwick.ac.uk

Ranko Lazić*
University of Warwick

r.s.lazic@warwick.ac.uk

Abstract

Adversarial reprogramming, introduced by Elsayed, Goodfellow, and Sohl-Dickstein, seeks to repurpose a neural network to perform a different task, by manipulating its input without modifying its weights. We prove that two-layer ReLU neural networks with random weights can be adversarially reprogrammed to achieve arbitrarily high accuracy on Bernoulli data models over hypercube vertices, provided the network width is no greater than its input dimension. We also substantially strengthen a recent result of Phuong and Lampert on directional convergence of gradient flow, and obtain as a corollary that training two-layer ReLU neural networks on orthogonally separable datasets can cause their adversarial reprogramming to fail. We support these theoretical results by experiments that demonstrate that, as long as batch normalisation layers are suitably initialised, even untrained networks with random weights are susceptible to adversarial reprogramming. This is in contrast to observations in several recent works that suggested that adversarial reprogramming is not possible for untrained networks to any degree of reliability.

1 Introduction

Elsayed, Goodfellow, and Sohl-Dickstein [2019] proposed *adversarial reprogramming*: given a neural network \mathcal{N} which performs a task $F : X \rightarrow Y$ and given an adversarial task $G : \tilde{X} \rightarrow \tilde{Y}$, repurpose \mathcal{N} to perform G by finding mappings $h_{\text{in}} : \tilde{X} \rightarrow X$ and $h_{\text{out}} : Y \rightarrow \tilde{Y}$ such that $G \approx h_{\text{out}} \circ F \circ h_{\text{in}}$. They focused on a setting where F and G are image classification tasks, X consists of large images, \tilde{X} consists of small images, and h_{in} and h_{out} are simple and computationally inexpensive: $h_{\text{in}}(\tilde{x}) = p + \tilde{x}$ draws the input \tilde{x} at the centre of the *adversarial program* p , and h_{out} is a hard coded mapping from the class labels Y to the class labels \tilde{Y} . Then the challenge of adversarial reprogramming is to find p such that $h_{\text{out}} \circ F \circ h_{\text{in}}$ approximates well the adversarial task G .

Remarkably, Elsayed et al. [2019] showed that a range of realistic neural networks can be adversarially reprogrammed to perform successfully several tasks. They considered six architectures trained on ImageNet [Russakovsky, Deng, Su, Krause, Satheesh, Ma, Huang, Karpathy, Khosla, Bernstein, Berg, and Fei-Fei, 2015] and found adversarial programs that achieve very good accuracies on a counting task, MNIST [LeCun, Bottou, Bengio, and Haffner, 1998], and CIFAR-10 [Krizhevsky, 2009]. In addition to the basic setting, they investigated limiting the visibility of the adversarial program by restricting its size or scale, or even concealing both the input and the adversarial program by hiding them within a normal image from ImageNet, and obtained good results.

Adversarial reprogramming can be seen as taking the crafting of adversarial examples [Biggio, Corona, Maiorca, Nelson, Šrndić, Laskov, Giacinto, and Roli, 2013, Szegedy, Zaremba, Sutskever, Bruna, Erhan, Goodfellow, and Fergus, 2014] to a next level. Like the universal adversarial perturbation of Moosavi-Dezfooli, Fawzi, Fawzi, and Frossard [2017], a single adversarial program is combined with every input from the adversarial task, but in contrast to the former where the goal is to cause natural images to be

*Equal contributions.

misclassified with high probability, adversarial reprogramming seeks a high accuracy of classification for the given adversarial task.

Adversarial reprogramming is also related to transfer learning [Raina, Battle, Lee, Packer, and Ng, 2007, Mesnil, Dauphin, Glorot, Rifai, Bengio, Goodfellow, Lavoie, Muller, Desjardins, Warde-Farley, Vincent, Courville, and Bergstra, 2011], however with important differences. Whereas transfer learning methods use the knowledge obtained from one task as a base for learning to perform another, and allow model parameters to be changed for the new task, in adversarial reprogramming the new task may bear no similarity with the old, and the model may not be altered but has to be manipulated through its input.

The latter features are suggestive of potential nefarious uses of adversarial reprogramming, and Elsayed et al. [2019] list several, such as repurposing computational resources to perform a task which violates the ethics code of system providers. However, its further explorations have demonstrated utility for virtuous deployments to medical image classification [Tsai, Chen, and Ho, 2020], natural language processing [Hambardzumyan, Khachatrian, and May, 2021, Neekhara, Hussain, Dubnov, and Koushanfar, 2019, Neekhara, Hussain, Du, Dubnov, Koushanfar, and McAuley, 2022], molecule toxicity prediction [Vinod, Chen, and Das, 2020], and time series classification [Yang, Tsai, and Chen, 2021]. In the last three works, adversarial reprogramming was achieved between different domains, e.g. repurposing neural networks trained on ImageNet to perform classification of DNA sequences, and of natural language sentiments and topics.

In spite of the variety of fruitful applications, it is still largely a mystery when adversarial reprogramming is possible and why. In the only work in this direction, Zheng, Feng, Xia, Jiang, Demontis, Pintor, Biggio, and Roli [2021] proposed the alignment $\|g\|_1 / (1/n \sum_i \|g_i\|_1)$ of the gradients g_i of the inputs from the adversarial task with their average g as the main indication of whether adversarial reprogramming will succeed. However, their experiments did not show a significant correlation between accuracy after reprogramming and the gradient alignment before reprogramming. The correlation was statistically significant with the gradient alignment after reprogramming, but that is unsurprising and it is unclear how to use it for predicting success.

Specifically, a central question on adversarial reprogramming is:

Can neural networks with random weights be adversarially reprogrammed, and more generally, how does training impact adversarial reprogrammability?

First, addressing this question is important for assessing scope of two claims made in the literature:

“[Adversarial] reprogramming usually fails when applied to untrained networks” [Zheng et al., 2021]. In addition to networks trained on ImageNet, Elsayed et al. [2019] experimented using the same architectures untrained, i.e. with random weights, and obtained generally poor results. Similarly, the experimental results of Neekhara et al. [2019] and Zheng et al. [2021] for random networks are significantly worse than their experimental results for trained networks. However, they remarked that this was surprising given the known richness of random networks (see e.g. He, Wang, and Hopcroft [2016c], Lee, Bahri, Novak, Schoenholz, Pennington, and Sohl-Dickstein [2018]), and that it was possibly due to simple reasons such as poor scaling of the random weights.

“The original task the neural networks perform is important for adversarial reprogramming” [Elsayed et al., 2019]. Nevertheless a number experimental results including those of Tsai et al. [2020], Neekhara et al. [2022], Vinod et al. [2020], Yang et al. [2021], Zheng et al. [2021] demonstrated successful adversarial reprogramming between tasks that are seemingly unrelated (e.g. repurposing networks trained on ImageNet to acts as HCL2000 [Zhang, Guo, Chen, and Li, 2009] classifiers) or from different domains, so the interaction between the original and adversarial tasks remains unclear.

Second, it is important due to implications for the following two applied considerations:

Disentangling architecture and training as factors in adversarial reprogrammability. Clarifying the respective bearings on adversarial reprogramming success of the network architecture and of the task

(if any) it was trained for would improve decision making, either to maximise the success in beneficial scenarios or to minimise it in detrimental ones.

Managing the cost of adversarial reprogramming. Understanding when training the network is not essential, and when training for longer does not help or even hinders adversarial reprogrammability, should make it possible to control better the economic and environmental costs.

1.1 Our contributions

We initiate a theoretical study of adversarial reprogramming. We focus on two-layer neural networks with ReLU activation, and on adversarial tasks given by the Bernoulli distributions of Schmidt, Santurkar, Tsipras, Talwar, and Mądry [2018] over hypercube vertices. The latter are binary classification data models in which the two classes are represented by opposite hypercube vertices, and when sampling a datapoint for a given class, we flip each coordinate of the corresponding class vertex with a certain probability. This probability is a parameter that controls the difficulty of the classification task. These data models are inspired by the MNIST dataset because MNIST images are close to binary (many pixels are almost fully black or white). The remaining parameters are the radius of the hypercube, the input dimension of the neural network, and its width.

We prove that, in this setting, for networks with random weights, adversarial programs exist that achieve arbitrarily high accuracy on the Bernoulli adversarial tasks. This holds for a wide variety of parameter regimes, provided the network width is no greater than its input dimension. The adversarial programs we construct depend on the weights of the network and on the class vertices (i.e., the direction) of the Bernoulli data model, and their Euclidean length is likely to be close to the square root of the input dimension.

We also prove that, in the same setting, training the network on orthogonally separable datasets can cause adversarial reprogramming to fail. Phuong and Lampert [2021] recently showed that, under several assumptions, training a two-layer ReLU network on such datasets by gradient flow makes it converge to a linear combination of two maximum-margin neurons. We provide a simpler proof of a significantly stronger result: we show that their assumptions of small initialisation, and of positive and negative support examples spanning the whole space, are not needed; and we generalise to the exponential loss function as well as the logistic one. We then observe that, for any Bernoulli data model whose direction is in a half-space of the difference of the maximum-margin neurons, and for any adversarial program, the accuracy tends to $1/2$ (i.e. approaches guessing) under a mild assumption on the growth rate of the difficulty of the data model.

In the experimental part of our work, we demonstrate that, as long as batch normalisation layers are suitably initialised, even untrained networks with random weights are susceptible to adversarial reprogramming. Our experiments are conducted with six realistic network architectures and MNIST as the adversarial task. We investigate two different schemes to combine input images with adversarial programs: replacing the centre of the program by the image as was done by Elsayed et al. [2019], and scaling the image to the size of the program and then taking a convex combination of the two. Each of the two schemes has a ratio parameter, and we explore their different values. We find that the second scheme gives better results in our experiments, and that for some choices of the ratio parameter, the accuracies on the test set across all six architectures are not far below what Elsayed et al. [2019] reported for networks trained on ImageNet.

1.2 Related works

Here we outline relations with several other works not already discussed.

Understanding adversarial examples. Adversarial reprogramming can be seen as a challenging type of adversarial attack. Instead of finding perturbations that push examples over a classification boundary,

the goal is to find an adversarial program which is an offset that, when added to any input from the adversarial task, with high probability makes it classified as desired. Equivalently, adversarial reprogramming seeks a single perturbation that pushes all inputs from the adversarial task to their respective target classes. Therefore understanding when and why neural networks are susceptible to adversarial reprogramming is an interesting piece of the puzzle of understanding adversarial examples. For example, our results on random networks suggest that sensitivity to well-generalising features in training data, which was identified by Ilyas, Santurkar, Tsipras, Engstrom, Tran, and Madry [2019] as a key cause of adversarial vulnerability, does not fully explain susceptibility to adversarial reprogramming. A different conceptual framework for understanding adversarial examples, in terms of a dimpled manifold model, was proposed by Shamir, Melamed, and BenShmuel [2021]; here our result that training for longer can be a defence against adversarial reprogramming suggests that it may be interesting to explore how its success depends on shapes of the dimples in classification boundaries as they evolve during training.

More directly related to our work are the results of Bartlett, Bubeck, and Cherapanamjeri [2021] who, building on the works of Daniely and Shacham [2020] and Bubeck, Cherapanamjeri, Gidel, and Tachet des Combes [2021], proved that random ReLU networks of constant depth have small adversarial perturbations that can be found in one step along the direction opposite to the input gradient. Those were advanced further recently by Montanari and Wu [2022], removing a restriction on layer widths. In comparison, our results show existence of adversarial programs that are points where the classification boundary behaves approximately as required for the adversarial task, and are sensitive to the radius and the difficulty of the latter as parameters; however we leave theoretical investigations of obtaining adversarial programs by gradient methods for future work.

Implicit bias of gradient descent. By showing that, for linear logistic regression on linearly separable data, gradient descent always converges to the maximum-margin solution, Soudry, Hoffer, Nacson, Gunasekar, and Srebro [2018] initiated a fruitful research direction on implicit bias of gradient descent, which tackles one of the greatest open questions in deep learning: why do overparameterised deep neural networks generalise well [Zhang, Bengio, Hardt, Recht, and Vinyals, 2017].

Some of the works closest to ours are: Lyu and Li [2020], Ji and Telgarsky [2020], who established that, for positively homogeneous deep networks and either exponential or logistic loss, if at some time training attains perfect accuracy and a small loss, then continuing the training makes the loss converge to 0 and the weights converge in direction to a Karush-Kuhn-Tucker point of a constrained optimisation problem on margin maximisation; Phuong and Lampert [2021], who showed that, from small and balanced initialisations, and when trained with logistic loss on orthogonally separable data whose positive and negative support examples span the whole space, two-layer ReLU networks converge to a linear combination of two maximum-margin neurons; Lyu, Li, Wang, and Arora [2021], who proved that, from small initialisations, and when trained with logistic loss on symmetric linearly separable data, two-layer networks with the leaky ReLU activation converge to a globally maximum-margin linear classifier, and that the result is fragile with respect to the symmetry assumption; and Vardi, Yehudai, and Shamir [2022], who showed that, for two-layer ReLU networks with first-layer biases and for data whose points are neither too many nor too correlated, if training converges then it produces non-robust solutions in spite of robust ones existing. To supplement our discussion above of the motivations for considering random versus trained networks in this work, we remark that we see merit in the point of Vardi et al. [2022] that *“trained networks are clearly not random, and properties that hold in random networks may not hold in trained networks.”*

Physical adversarial examples. Currently more distant but with potential for interesting connections to our work is the vibrant research direction on adversarial examples in the physical world. For example, our results may inform attempts to design adversarial accessories with prescribed effects for a set of participants [Sharif, Bhagavatula, Bauer, and Reiter, 2016], or adversarial patches that cause prescribed classifications for a set of objects [Brown, Mané, Roy, Abadi, and Gilmer, 2017].

2 Random networks

Basic notations. We write: $[n]$ for the set $\{1, \dots, n\}$, $\|\mathbf{v}\|$ for the Euclidean length of a vector \mathbf{v} , $\angle(\mathbf{v}, \mathbf{v}')$ for the angle between \mathbf{v} and \mathbf{v}' , and \mathbb{H}^d for the d -dimensional unit hypercube $\{\pm 1/\sqrt{d}\}^d$.

Two-layer ReLU networks. We consider two-layer neural networks \mathcal{N} with the ReLU activation. We write d for the input dimension, k for the width, $\mathbf{w}_1, \dots, \mathbf{w}_k \in \mathbb{R}^d$ for the weights of the first layer, and $a_1, \dots, a_k \in \mathbb{R}$ for the weights of the second layer. For an input $\mathbf{x} \in \mathbb{R}^d$, the output is thus

$$\mathcal{N}(\mathbf{x}) := \sum_{j=1}^k a_j \psi(\mathbf{w}_j^\top \mathbf{x}),$$

where $\psi(u) = \max\{u, 0\}$ is the ReLU function.

Random weights. In this section, we assume that the weights in \mathcal{N} are random as follows:

- each \mathbf{w}_j consists of d independent centred Gaussians with variance $1/d$, and
- each a_j is independently uniformly distributed in $\{\pm 1/\sqrt{k}\}$.

This distribution is as in Bubeck et al. [2021], and standard for theoretical investigations. It is similar to He’s initialisation [He, Zhang, Ren, and Sun, 2015], with the second layer discretised for simplicity.

The variances of the weights are such that, for any input $\mathbf{x} \in \mathbb{R}^d$ of Euclidean length \sqrt{d} , each $\mathbf{w}_j^\top \mathbf{x}$ is a standard Gaussian, and for large widths k the distribution of $\mathcal{N}(\mathbf{x})$ is close to centred Gaussian with variance $1/2$.

Bernoulli data models. Adapting from Schmidt et al. [2018], given a hypercube vertex $\phi \in \mathbb{H}^d$, a radius $\rho > 0$, and a class bias parameter $0 < \tau \leq 1/2$, we define the (ϕ, ρ, τ) -Bernoulli distribution over $(\mathbf{x}, y) \in \rho\mathbb{H}^d \times \{\pm 1\}$ as follows:

- first draw the label y uniformly at random from $\{\pm 1\}$,
- then sample the data point \mathbf{x} by taking $y\rho\phi$ and flipping the sign of each coordinate independently with probability $1/2 - \tau$.

These binary classification data models on hypercube vertices are inspired by the MNIST dataset [LeCun et al., 1998]. The class bias parameter τ controls the difficulty of the classification task, which increases as τ tends to zero, i.e. as $1/\tau$ tends to infinity.

Adversarial program. In this section, we assume that $k \leq d$, i.e. the network width is no greater than the input dimension, and we define an adversarial program \mathbf{p} which depends on the weights of the network \mathcal{N} and on the direction ϕ of the Bernoulli data model.

With probability 1, for all $j \in [k]$, we have that $a_j \mathbf{w}_j^\top \phi \neq 0$. Let us write K^+ for $\{j \in [k] \mid a_j \mathbf{w}_j^\top \phi > 0\}$, and K^- for $\{j \in [k] \mid a_j \mathbf{w}_j^\top \phi < 0\}$. Then, for all $j \in [k]$, let:

$$\mathbf{p}'_j = \begin{cases} 0 & \text{if } j \in K^+, \\ -\sqrt{d/|K^-|} & \text{if } j \in K^-. \end{cases}$$

Since $k \leq d$, with probability 1, the weights vectors \mathbf{w}_j are linearly independent, i.e. the $k \times d$ matrix \mathbf{W} whose rows are \mathbf{w}_j has a positive smallest singular value $s_{\min}(\mathbf{W})$. Hence $\mathbf{p} \in \mathbb{R}^d$ exists such that

$$\mathbf{p}' = \mathbf{W}\mathbf{p} \quad \text{and} \quad \frac{\|\mathbf{p}'\|}{s_{\max}(\mathbf{W})} \leq \|\mathbf{p}\| \leq \frac{\|\mathbf{p}'\|}{s_{\min}(\mathbf{W})}. \quad (1)$$

The neurons in K^+ can be thought of as “helpful” for the adversarial task, and those in K^- as “unhelpful”. This definition of an adversarial program \mathbf{p} ensures that its effect is to introduce as first-layer biases the entries of the vector \mathbf{p}' . They are 0 (i.e. do nothing) for every “helpful” neuron, and the negative value $-\sqrt{d/|K^-|}$ (i.e. reduce the contribution to the network output) for every “unhelpful” neuron.

From the inequalities in (1), we can expect $\|\mathbf{p}\| \approx \sqrt{d}$ if $k = o(d)$ (see Appendix A for details).

Expected reprogramming accuracy. Our main result in this section provides a lower (respectively, upper) bound on the output of the adversarially reprogrammed network for positively (respectively, negatively) labelled inputs sampled from the Bernoulli data model. The proof, which proceeds by analysing concentrations of the underlying distributions, can be found in Appendix B.

Theorem 1. *There exist constants C_1, C_2, C_3, C_4 and C_5 such that, with probability at least $(1 - C_1\gamma)(1 - \gamma^\dagger)$ over the choice of the network \mathcal{N} and the labelled data point (\mathbf{x}, y) sampled from the (ϕ, ρ, τ) -Bernoulli distribution, provided that $2d\tau^2 \geq \ln(1/\gamma^\dagger)$, we have*

$$y\mathcal{N}(\mathbf{p} + \mathbf{x}) > \frac{\sqrt{k}\rho}{\sqrt{d}} \left(C_2\tau - C_3 \exp\left(-\frac{d^2}{2k\rho^2}\right) \min\left\{1, \frac{k\rho^2}{d^2}\right\} - C_4\sqrt{\frac{\ln(1/\gamma)}{k}} - C_5\sqrt{\frac{\ln(1/\gamma^\dagger)}{d}} \right).$$

A corollary is that, for sufficiently large input dimensions d , and under mild restrictions on the growth rates of the network width k , and the radius ρ and the difficulty $1/\tau$ of the Bernoulli data model, expected reprogramming accuracy is at least $(1 - C_1\gamma)(1 - \gamma^\dagger)$, which by tuning the probability parameters γ and γ^\dagger can be arbitrarily close to 100%. The growth rate restrictions indicate that networks with smaller widths can be reprogrammed for tasks with larger radii, but that networks with larger widths can be reprogrammed for tasks that are more difficult. The proof is in Appendix B.

Corollary 2. *Suppose that*

$$k = \Omega(d^{\eta(k)}), \quad \rho = O(d^{\eta(\rho)}), \quad 1/\tau = O(d^{\eta(\tau)}) \quad \text{and} \quad 1/\tau = \omega_d(1),$$

where $\eta(k), \eta(\rho), \eta(\tau) \in [0, 1]$ are arbitrary constants that satisfy

$$\eta(\rho) < 1 - \eta(k)/2 \quad \text{and} \quad \eta(\tau) < \eta(k)/2.$$

Then, for sufficiently large input dimensions d , the expected accuracy of the adversarially reprogrammed network \mathcal{N} on the (ϕ, ρ, τ) -Bernoulli data model is arbitrarily close to 100%.

3 Implicit bias

Orthogonally separable dataset. In this section, we consider training the network on a binary classification dataset $S = \{(\mathbf{x}_1, y_1), \dots, (\mathbf{x}_n, y_n)\} \subseteq \mathbb{R}^d \times \{\pm 1\}$ which is orthogonally separable [Phuong and Lampert, 2021], i.e. for all $i, i' \in [n]$ we have:

$$\mathbf{x}_i^\top \mathbf{x}_{i'} > 0 \quad \text{if} \quad y_i = y_{i'}, \quad \text{and} \quad \mathbf{x}_i^\top \mathbf{x}_{i'} \leq 0 \quad \text{if} \quad y_i \neq y_{i'}.$$

In other words, every data point can act as a linear separator, although some data points from the opposite class may be exactly orthogonal to it.

Gradient flow with exponential or logistic loss. For two-layer ReLU networks with input dimension d and width k as before (but without the assumption $k \leq d$, which is not needed in this section), we denote the vector of all weights by

$$\boldsymbol{\theta} := (\mathbf{w}_1, \dots, \mathbf{w}_k, a_1, \dots, a_k) \in \mathbb{R}^{k(d+1)},$$

and we write \mathcal{N}_θ for the network whose weights are the coordinates of the vector $\boldsymbol{\theta}$.

The empirical loss of \mathcal{N}_θ on S is $\mathcal{L}(\theta) := \sum_{i=1}^n \ell(y_i \mathcal{N}_\theta(\mathbf{x}_i))$, where ℓ is either the exponential $\ell_{\text{exp}}(u) = e^{-u}$ or the logistic $\ell_{\text{log}}(u) = \ln(1 + e^{-u})$ loss function.

A trajectory of gradient flow is a function $\theta(t) : [0, \infty) \rightarrow \mathbb{R}^{k(d+1)}$ that is an arc, i.e. it is absolutely continuous on every compact subinterval, and that satisfies the differential inclusion

$$\frac{d\theta}{dt} \in -\partial\mathcal{L}(\theta(t)) \quad \text{for almost all } t \in [0, \infty),$$

where $\partial\mathcal{L}$ denotes the Clarke subdifferential [Clarke, 1975] of the locally Lipschitz function \mathcal{L} .

Gradient flow is gradient descent with infinitesimal step size. We work with the Clarke subdifferential in order to handle the non-differentiability of the ReLU function at zero: $\partial\psi(0)$ is the whole interval $[0, 1]$. At points of continuous differentiability, the Clarke subdifferential amounts to the gradient, e.g. $\partial\mathcal{L}(\theta) = \{\nabla\mathcal{L}(\theta)\}$. For some further background, see Appendix C.

Initialisation of network weights. In this section, we assume that the initialisation is

balanced: for all $j \in [k]$, at time $t = 0$ we have $|a_j| = \|\mathbf{w}_j\| > 0$; and

live: for both signs $s \in \{\pm 1\}$ there exist $i_s \in [n]$ and $j_s \in [k]$ such that $y_{i_s} = s$ and at time $t = 0$ we have $y_{i_s} a_{j_s} \psi(\mathbf{w}_{j_s}^\top \mathbf{x}_{i_s}) > 0$.

The balanced assumption has featured in previous work (see e.g. Phuong and Lampert [2021], Lyu et al. [2021]). It ensures that it remains to hold throughout the training, and that the signs of the second-layer weights a_j do not change (see the proof of Theorem 3). The live assumption (present probabilistically in Phuong and Lampert [2021]) is mild: it states that at least one positively initialised neuron is active for at least one positive input, and the same for negative ones.

Convergence of gradient flow. Our main result in this section establishes that the early phase of training necessarily reaches a point where the empirical loss is less than $\ell(0)$, which implies that then every input is classified correctly by the network. Perhaps surprisingly, no small initialisation assumption is needed, however the proof makes extensive use of orthogonal separability of the dataset (see Appendix E, which contains all proofs for this section).

Theorem 3. *There exists a time t_0 such that $\mathcal{L}(\theta(t_0)) < \ell(0)$.*

This enables us to apply to the late phase recent results of Lyu and Li [2020], Ji and Telgarsky [2020], Lyu et al. [2021] and obtain the next corollary, which is significantly stronger than the main result of Phuong and Lampert [2021], extending it to exponential loss, and showing that assumptions of small initialisation, and of positive and negative support examples spanning the whole space, are not needed. The corollary establishes that each neuron converges to one of three types: a scaling of the maximum-margin vector for the positive data class, a scaling of the maximum-margin vector for the negative data class, or zero. The two maximum-margin vectors are defined as follows: for both signs $s \in \{\pm 1\}$, let $I_s := \{i \in [n] \mid y_i = s\}$, and let \mathbf{v}_s be the unique minimiser of the quadratic problem

$$\text{minimise } \frac{1}{2} \|\mathbf{v}\|^2 \quad \text{subject to } \forall i \in I_s : \mathbf{v}^\top \mathbf{x}_i \geq 1.$$

That a trajectory $\theta(t)$ converges in direction to a vector $\tilde{\theta}$ means $\lim_{t \rightarrow \infty} \theta(t) / \|\theta(t)\| = \tilde{\theta} / \|\tilde{\theta}\|$.

Corollary 4. *As the time tends to infinity, we have that the empirical loss converges to zero, the Euclidean norm of the weights converges to infinity, and the weights converge in direction to some θ such that for all $j \in [k]$ we have $|a_j| = \|\mathbf{w}_j\|$, and if $a_j \neq 0$ then*

$$\frac{\mathbf{w}_j}{\|\mathbf{w}_j\|} = \frac{\mathbf{v}_{\text{sgn}(a_j)}}{\sum_{\text{sgn}(a_{j'}) = \text{sgn}(a_j)} a_{j'}^2}.$$

Thanks to homogeneity, the sign of the network output does not depend on the norm of the weights, only on their direction. Examining networks whose weights are directional limits as in Corollary 4 is therefore informative of consequences for adversarial reprogramming of training to infinity. The following results tell us that, for any Bernoulli data model whose direction is in a half-space of the difference of the maximum-margin vectors, and for any adversarial program, the accuracy tends to $1/2$ provided that the difficulty $1/\tau$ of the data model increases slower than the square root of the input dimension d . The latter assumption is considerably weaker than in the results of Schmidt et al. [2018] on the Bernoulli data model, where the bound is in terms of the fourth root. The statement also tells us that this failure cannot be fixed by choosing in advance a different mapping from the class labels of the original task to the class labels of the adversarial task. Since we consider binary classification tasks here, the mapping can be represented by a multiplier $m \in \{\pm 1\}$.

Proposition 5. *Suppose weights θ are as in Corollary 4, class label mapping $m \in \{\pm 1\}$ is arbitrary, data model \mathcal{D} is any (ϕ, ρ, τ) -Bernoulli distribution such that $m \cos \angle(\mathbf{v}_1 - \mathbf{v}_{-1}, \phi) < 0$, and adversarial program \mathbf{p} is arbitrary. Then we have that*

$$\mathbb{P}_{(\mathbf{x}, y) \sim \mathcal{D}}\{m y \mathcal{N}_{\theta}(\mathbf{p} + \mathbf{x}) > 0\} \leq \frac{1}{2} + \frac{1}{2} e^{-2d\tau^2 \cos^2 \angle(\mathbf{v}_1 - \mathbf{v}_{-1}, \phi)}.$$

4 Experiments

Network architectures and initialisation. Our experiments are conducted using the following six network architectures: ResNet-50 [He, Zhang, Ren, and Sun, 2016a], ResNet-50V2, ResNet-101V2, ResNet-152V2 [He, Zhang, Ren, and Sun, 2016b], Inception-v3 [Szegedy, Vanhoucke, Ioffe, Shlens, and Wojna, 2016], and EfficientNet-B0 [Tan and Le, 2019].

We use the networks exactly as implemented in Keras in TensorFlow 2.8.0 including the method for randomly initialising the trainable weights. For biases, this means they are initialised with 0. For all other trainable weights, mostly, the Xavier uniform initialiser [Glorot and Bengio, 2010] is used in this implementation. EfficientNet is an exception, where many layers instead use a truncated normal distribution that has mean 0 and standard deviation $\sqrt{2}$ /number of output units.

All of these networks involve batch normalisation layers [Ioffe and Szegedy, 2015]. Every such layer maintains a moving mean and a moving variance based on batches it has seen during training. The inputs are then normalised accordingly: they are shifted by the recorded mean and scaled by the inverse of the recorded variance. Note that the moving mean and variance values are not trainable, i.e., they are not subject to updates by the optimiser during training. During inference, the moving mean and variance values are no longer updated, and the normalisation is performed based on the last values recorded during training.

Crucially, in the default implementation of these networks, these moving mean and moving variance values are initialised as 0 and 1, respectively. Therefore, an untrained network initialised in this way will behave as if the batch normalisation layers were not present.

To obtain more sensible random networks, i.e., ones that can still make use of batch normalisation, we initialise the moving mean and variance of batch normalisation layers differently. We generate a batch of 100 random images (each pixel value is chosen independently and uniformly at random in the allowed range). This single batch is then fed through the random network and each batch normalisation layer records the mean and variance values it sees at its input (and normalises its output accordingly). The trainable weights of the network are not changed during this process.

We should note that, in addition to the moving mean and variance, batch normalisation layers can have *trainable* weights, by means of which the output mean and variance can be tuned. Specifically, such a layer may have trainable weights γ and β , and will scale its otherwise normalised output by γ and shift it by β . If present, these trainable weights are initialised as 1 and 0 respectively, and hence have no effect.

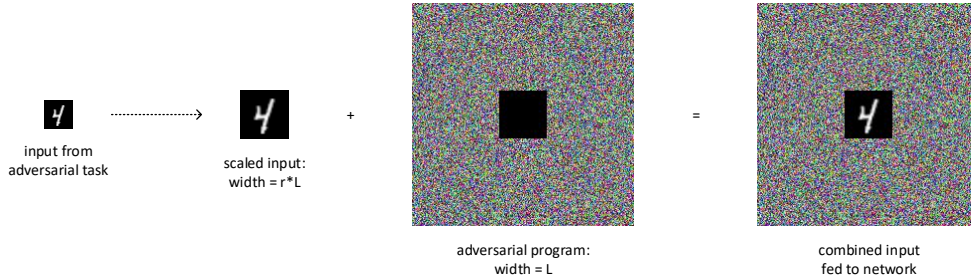


Figure 1: Scheme 1 for combining input images with adversarial programs. In this example, the width and height of the adversarial program are 224 and the parameter r equals $2^{-20/9} \approx 0.214$, so the input image is scaled to width and height $r \cdot 224$ rounded, which is 48.

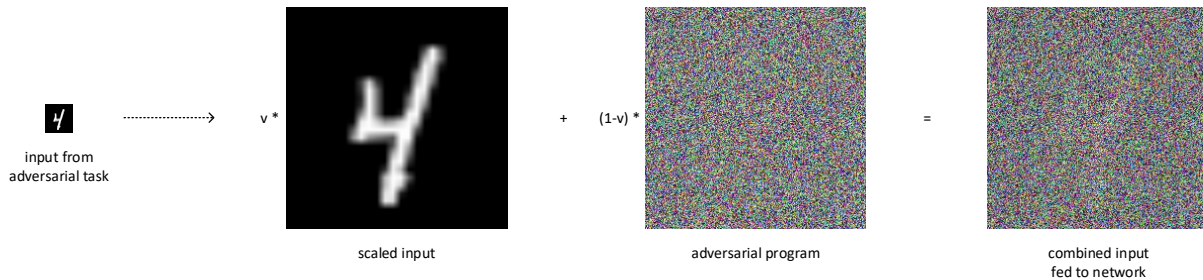


Figure 2: Scheme 2 for combining input images with adversarial programs. In this example, the sizes of the scaled input image and the adversarial program are 224×224 . The parameter v equals $2^{-40/9} \approx 0.046$, so the weight of the input image in the convex combination with the adversarial program is approximately 4.6%, which makes it faintly visible.

Our initialisation procedure does not modify these trainable weights and they are therefore not used in our random networks.

Combining input images with adversarial programs. Our adversarial programs are colour images whose sizes match the expected input size of the networks. This is 224×224 for all networks except Inception-v3, where it is 299×299 .

We use two different schemes to combine input images with the adversarial program. The first scheme, used by Elsayed et al. [2019], is to take the adversarial program and overwrite a portion of it by the input image. We do this in such a way that the input image is, up to rounding, centred in the adversarial program. We can vary the construction by scaling the input image up or down before applying this procedure. In particular, we use a parameter $r \in [0, 1]$ and scale the input image, using bilinear interpolation, in such a way that r times the width of the adversarial program is equal to the width of the scaled image. That we focus on the width is not important because all our inputs and programs are square. An illustration is shown in Figure 1.

Our second scheme involves scaling the image to the same size as the adversarial program and then taking a convex combination of the two. We use a parameter $v \in [0, 1]$ to specify how much weight the input image should get in this convex combination. Specifically, the combined image is obtained by calculating $v \cdot I + (1 - v) \cdot P$, where I is the input image and P is the adversarial program. An illustration is shown in Figure 2.

Adversarial task dataset. Elsayed et al. [2019] evaluate adversarial reprogramming on random net-

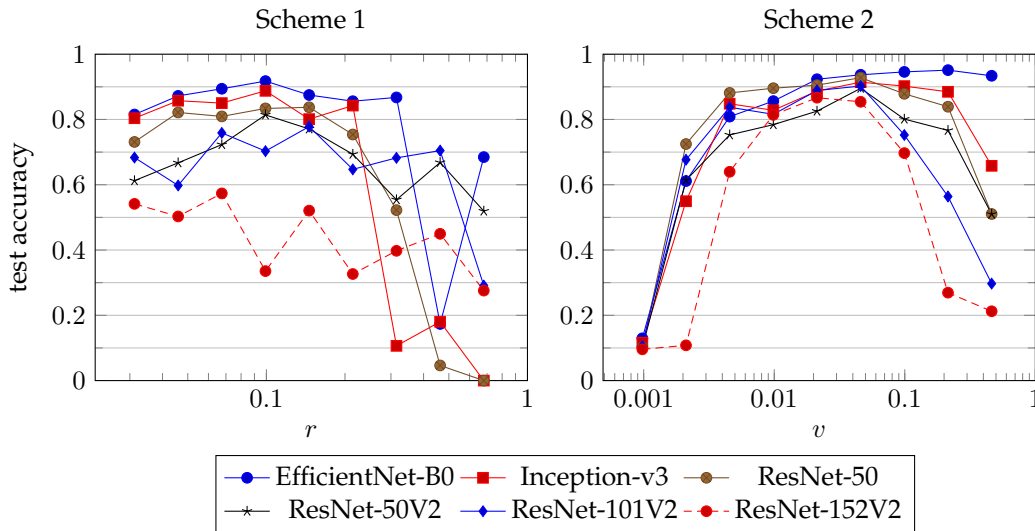


Figure 3: The accuracy achieved by the adversarial program on the test set for different parameters of the two schemes of combining input images with adversarial programs. The horizontal axes are logarithmic. The data for the plots is listed in Appendix F.

works using the MNIST dataset. In other words, they were asking whether it is possible to repurpose a random network for the task of classifying the handwritten digits from the MNIST dataset. We use the same dataset, which consists of 60,000 training images and 10,000 test images, for our experiments. It is available under the Creative Commons Attribution-Share Alike 3.0 licence.

The networks we use classify inputs into 1,000 classes. We map the 10 labels of the MNIST dataset onto the first 10 of these classes.

Finding adversarial programs. Internally, we represent adversarial programs using unconstrained weights. We then apply a softsign function to the weights to map them into the range $(-1, 1)$, and further shift and scale the program such that the pixel values lie in the same range that is used for the input images. The program is initialised in such a way that after the application of the softsign function, each value lies uniformly at random in $(-1, 1)$. We use the 60,000 training images to run an Adam optimiser [Kingma and Ba, 2015] with learning rate 0.01 and a batch size of 100 to optimise the unconstrained weights of the adversarial program. We report the accuracy on the 10,000 test images after 20 epochs, please see Figure 3. The experiments were run on a standard desktop computer with two NVIDIA GeForce RTX 3080 Ti GPUs.

We did not explore other optimisers, batch sizes, and learning rates, since our first choices already resulted in suitable adversarial programs for these random networks. However, we did explore the two different schemes of combining input images with adversarial programs, and different values for the respective parameters r and v . For each network, and each value of r and v , we ran a single experiment. While averaging over multiple experiments could potentially reduce the noise in the results, due to the tests for different values of r and v , an overall picture emerges even when running one experiment per data point.

Discussion. Overall, the second scheme of combining input images with adversarial programs appears to give better and more reliable results in our experiments. For both schemes, the choice of parameters is important. Clearly, when r or v is 0, the input image is not visible to the network at all. On the other hand, when r or v is 1, there no longer is an adversarial program. In most cases, best results are achieved when the adversarial program is significantly larger (either by actual size in the first scheme, or in terms of pixel value ranges in the second scheme) than the input image.

In the second scheme in particular, we see accuracies on the test set which are lower, but not much lower than what Elsayed et al. [2019] reported for networks trained on ImageNet. For $v \approx 0.046$ for example, we see accuracies of 93.7%, 92.8%, 91.4%, 90.2%, 89.5%, 85.4% for EfficientNet-B0, ResNet-50, Inception-v3, ResNet-101V2, ResNet-50V2, ResNet-152V2, respectively. This suggests that, while training, say, on ImageNet may impact the possibility of finding suitable adversarial programs, such a training may be less important than previously thought and other factors are of significant importance.

References

- Peter L. Bartlett, Sébastien Bubeck, and Yeshwanth Cherapanamjeri. Adversarial Examples in Multi-Layer Random ReLU Networks. In *NeurIPS*, pages 9241–9252, 2021. 4
- Battista Biggio, Igino Corona, Davide Maiorca, Blaine Nelson, Nedim Šrndić, Pavel Laskov, Giorgio Giacinto, and Fabio Roli. Evasion Attacks against Machine Learning at Test Time. In *ECML PKDD*, pages 387–402, 2013. 1
- Tom B. Brown, Dandelion Mané, Aurko Roy, Martín Abadi, and Justin Gilmer. Adversarial Patch. *CoRR*, abs/1712.09665, 2017. 4
- Sébastien Bubeck, Yeshwanth Cherapanamjeri, Gauthier Gidel, and Rémi Tachet des Combes. A single gradient step finds adversarial examples on random two-layers neural networks. In *NeurIPS*, pages 10081–10091, 2021. 4, 5
- Frank H. Clarke. Generalized gradients and applications. *Transactions of the American Mathematical Society*, 205: 247–262, 1975. 7, 18
- Amit Daniely and Hadas Shacham. Most ReLU Networks Suffer from ℓ^2 Adversarial Perturbations. In *NeurIPS*, 2020. 4
- Damek Davis, Dmitriy Drusvyatskiy, Sham M. Kakade, and Jason D. Lee. Stochastic Subgradient Method Converges on Tame Functions. *Found. Comput. Math.*, 20(1):119–154, 2020. 19
- Joydeep Dutta, Kalyanmoy Deb, Rupesh Tulshyan, and Ramnik Arora. Approximate KKT points and a proximity measure for termination. *J. Glob. Optim.*, 56(4):1463–1499, 2013. 18
- Gamaleldin F. Elsayed, Ian Goodfellow, and Jascha Sohl-Dickstein. Adversarial Reprogramming of Neural Networks. In *ICLR*, 2019. 1, 2, 3, 9, 11
- Xavier Glorot and Yoshua Bengio. Understanding the difficulty of training deep feedforward neural networks. In *AISTATS*, pages 249–256, 2010. 8
- Karen Hambardzumyan, Hrant Khachatryan, and Jonathan May. WARP: Word-level Adversarial ReProgramming. In *ACL/IJCNLP*, pages 4921–4933, 2021. 2
- Kaiming He, Xiangyu Zhang, Shaoqing Ren, and Jian Sun. Delving Deep into Rectifiers: Surpassing Human-Level Performance on ImageNet Classification. In *ICCV*, pages 1026–1034, 2015. 5
- Kaiming He, Xiangyu Zhang, Shaoqing Ren, and Jian Sun. Deep Residual Learning for Image Recognition. In *CVPR*, pages 770–778, 2016a. 8
- Kaiming He, Xiangyu Zhang, Shaoqing Ren, and Jian Sun. Identity Mappings in Deep Residual Networks. In *ECCV*, pages 630–645, 2016b. 8
- Kun He, Yan Wang, and John E. Hopcroft. A Powerful Generative Model Using Random Weights for the Deep Image Representation. In *NeurIPS*, pages 631–639, 2016c. 2
- Andrew Ilyas, Shibani Santurkar, Dimitris Tsipras, Logan Engstrom, Brandon Tran, and Aleksander Mądry. Adversarial Examples Are Not Bugs, They Are Features. In *NeurIPS*, pages 125–136, 2019. 4
- Sergey Ioffe and Christian Szegedy. Batch Normalization: Accelerating Deep Network Training by Reducing Internal Covariate Shift. In *ICML*, pages 448–456, 2015. 8
- Ziwei Ji and Matus Telgarsky. Directional convergence and alignment in deep learning. In *NeurIPS*, 2020. 4, 7, 21
- Diederik P. Kingma and Jimmy Ba. Adam: A Method for Stochastic Optimization. In *ICLR*, 2015. 10

- Alex Krizhevsky. Learning Multiple Layers of Features from Tiny Images. Master’s thesis, University of Toronto, 2009. 1
- Yann LeCun, Léon Bottou, Yoshua Bengio, and Patrick Haffner. Gradient-based learning applied to document recognition. *Proc. IEEE*, 86(11):2278–2324, 1998. 1, 5
- Jaehoon Lee, Yasaman Bahri, Roman Novak, Samuel S. Schoenholz, Jeffrey Pennington, and Jascha Sohl-Dickstein. Deep Neural Networks as Gaussian Processes. In *ICLR*, 2018. 2
- Kaifeng Lyu and Jian Li. Gradient Descent Maximizes the Margin of Homogeneous Neural Networks. In *ICLR*, 2020. 4, 7, 18, 21
- Kaifeng Lyu, Zhiyuan Li, Runzhe Wang, and Sanjeev Arora. Gradient Descent on Two-layer Nets: Margin Maximization and Simplicity Bias. In *NeurIPS*, pages 12978–12991, 2021. 4, 7, 22
- Grégoire Mesnil, Yann N. Dauphin, Xavier Glorot, Salah Rifai, Yoshua Bengio, Ian J. Goodfellow, Erick Lavoie, Xavier Muller, Guillaume Desjardins, David Warde-Farley, Pascal Vincent, Aaron C. Courville, and James Bergstra. Unsupervised and Transfer Learning Challenge: a Deep Learning Approach. In *ICML Workshop on Unsupervised and Transfer Learning*, pages 97–110, 2011. 2
- Andrea Montanari and Yuchen Wu. Adversarial Examples in Random Neural Networks with General Activations. *CoRR*, abs/2203.17209, 2022. 4
- Seyed-Mohsen Moosavi-Dezfooli, Alhussein Fawzi, Omar Fawzi, and Pascal Frossard. Universal Adversarial Perturbations. In *CVPR*, pages 86–94, 2017. 1
- Paarth Neekhara, Shehzeen Hussain, Shlomo Dubnov, and Farinaz Koushanfar. Adversarial Reprogramming of Text Classification Neural Networks. In *EMNLP-IJCNLP*, pages 5215–5224, 2019. 2
- Paarth Neekhara, Shehzeen Hussain, Jinglong Du, Shlomo Dubnov, Farinaz Koushanfar, and Julian J. McAuley. Cross-modal Adversarial Reprogramming. In *WACV*, pages 2898–2906, 2022. 2
- Mary Phuong and Christoph H. Lampert. The inductive bias of ReLU networks on orthogonally separable data. In *ICLR*, 2021. 3, 4, 6, 7, 19
- Rajat Raina, Alexis Battle, Honglak Lee, Benjamin Packer, and Andrew Y. Ng. Self-taught learning: transfer learning from unlabeled data. In *ICML*, pages 759–766, 2007. 2
- Olga Russakovsky, Jia Deng, Hao Su, Jonathan Krause, Sanjeev Satheesh, Sean Ma, Zhiheng Huang, Andrej Karpathy, Aditya Khosla, Michael S. Bernstein, Alexander C. Berg, and Li Fei-Fei. ImageNet Large Scale Visual Recognition Challenge. *Int. J. Comput. Vis.*, 115(3):211–252, 2015. 1
- Ludwig Schmidt, Shibani Santurkar, Dimitris Tsipras, Kunal Talwar, and Aleksander Mądry. Adversarially Robust Generalization Requires More Data. In *NeurIPS*, pages 5019–5031, 2018. 3, 5, 8, 16, 23
- Adi Shamir, Odelia Melamed, and Oriel BenShmuel. The Dimpled Manifold Model of Adversarial Examples in Machine Learning. *CoRR*, abs/2106.10151, 2021. 4
- Mahmood Sharif, Sruti Bhagavatula, Lujo Bauer, and Michael K. Reiter. Accessorize to a Crime: Real and Stealthy Attacks on State-of-the-Art Face Recognition. In *CCS*, pages 1528–1540, 2016. 4
- Daniel Soudry, Elad Hoffer, Mor Shpigel Nacson, Suriya Gunasekar, and Nathan Srebro. The Implicit Bias of Gradient Descent on Separable Data. *J. Mach. Learn. Res.*, 19:70:1–70:57, 2018. 4
- Christian Szegedy, Wojciech Zaremba, Ilya Sutskever, Joan Bruna, Dumitru Erhan, Ian J. Goodfellow, and Rob Fergus. Intriguing properties of neural networks. In *ICLR*, 2014. 1
- Christian Szegedy, Vincent Vanhoucke, Sergey Ioffe, Jonathon Shlens, and Zbigniew Wojna. Rethinking the Inception Architecture for Computer Vision. In *CVPR*, pages 2818–2826, 2016. 8
- Mingxing Tan and Quoc V. Le. EfficientNet: Rethinking Model Scaling for Convolutional Neural Networks. In *ICML*, pages 6105–6114, 2019. 8
- Yun-Yun Tsai, Pin-Yu Chen, and Tsung-Yi Ho. Transfer Learning without Knowing: Reprogramming Black-box Machine Learning Models with Scarce Data and Limited Resources. In *ICML*, pages 9614–9624, 2020. 2

- Gal Vardi, Gilad Yehudai, and Ohad Shamir. Gradient Methods Provably Converge to Non-Robust Networks. *CoRR*, abs/2202.04347, 2022. 4
- Roman Vershynin. Introduction to the non-asymptotic analysis of random matrices. In Yonina C. Eldar and Gitta Kutyniok, editors, *Compressed Sensing*, pages 210–268. Cambridge University Press, 2012. URL <http://arxiv.org/abs/1011.3027>. 13
- Roman Vershynin. *High-dimensional probability: An introduction with applications in data science*, volume 47 of *Cambridge Series in Statistical and Probabilistic Mathematics*. Cambridge University Press, 2018. 15, 16
- Ria Vinod, Pin-Yu Chen, and Payel Das. Reprogramming Language Models for Molecular Representation Learning. *CoRR*, abs/2012.03460, 2020. 2
- Martin J. Wainwright. *High-dimensional statistics: A non-asymptotic viewpoint*, volume 48 of *Cambridge Series in Statistical and Probabilistic Mathematics*. Cambridge University Press, 2019. 16
- Chao-Han Huck Yang, Yun-Yun Tsai, and Pin-Yu Chen. Voice2Series: Reprogramming Acoustic Models for Time Series Classification. In *ICML*, pages 11808–11819, 2021. 2
- Chiyuan Zhang, Samy Bengio, Moritz Hardt, Benjamin Recht, and Oriol Vinyals. Understanding deep learning requires rethinking generalization. In *ICLR*, 2017. 4
- Honggang Zhang, Jun Guo, Guang Chen, and Chun-Guang Li. HCL2000 - A Large-scale Handwritten Chinese Character Database for Handwritten Character Recognition. In *ICDAR*, pages 286–290, 2009. 2
- Yang Zheng, Xiaoyi Feng, Zhaoqiang Xia, Xiaoyue Jiang, Ambra Demontis, Maura Pintor, Battista Biggio, and Fabio Roli. Why Adversarial Reprogramming Works, When It Fails, and How to Tell the Difference. *CoRR*, abs/2108.11673, 2021. 2

A Length of the adversarial program

To estimate the length of the adversarial program defined in Section 2, we make use of the following known bounds on the smallest and largest singular values of matrices of independent identical Gaussians.

Theorem 6 (see e.g. Vershynin [2012, Corollary 5.35]). *Let \mathbf{A} be an $n \times m$ matrix whose entries are independent centred Gaussians with variance $1/d$. Then with probability at least $1 - \gamma$ its smallest and largest singular values satisfy*

$$\frac{\sqrt{m} - \sqrt{n} - \sqrt{2 \ln(2/\gamma)}}{\sqrt{d}} \leq s_{\min}(\mathbf{A}) \leq s_{\max}(\mathbf{A}) \leq \frac{\sqrt{m} + \sqrt{n} + \sqrt{2 \ln(2/\gamma)}}{\sqrt{d}}.$$

It follows that, in the regime $k = o(d)$, applying Theorem 6 to the $k \times d$ matrix \mathbf{W} with $\gamma = o_d(1)$ and $\gamma = e^{-o(d)}$ gives us that with probability $1 - o_d(1)$ the singular values are within $1 \pm o_d(1)$. Then, from the inequalities in (1), we have that $\|\mathbf{p}\|$ is close to $\|\mathbf{p}'\|$ for large d . Observe that $\|\mathbf{p}'\| = \sqrt{d}$ whenever K^- is not empty, which occurs with probability $1 - 2^{-k}$ because the events $\{j \in K^-\}$ are independent and have probability $1/2$.

B Proofs for random networks

Here we work with the notations and assumptions from Section 2, so we have: a random two-layer ReLU network \mathcal{N} with input dimension d , width k such that $k \leq d$, and weights w_j and a_j for $j \in [k]$; a (ϕ, ρ, τ) -Bernoulli data model; and an adversarial program \mathbf{p} defined as in (1).

First we prove a lemma that provides a lower (respectively, upper) bound on the sum of outputs of the “helpful” neurons for the adversarial program \mathbf{p} together with inputs \mathbf{x} that are positively (respectively, negatively) correlated with the direction ϕ of the data model. In the proof, we use concentration properties of the weights of \mathcal{N} to show that these neurons get close to computing together the inner product $\phi^\top \mathbf{x}$, which equals $\rho \cos \alpha$ where α is the angle between ϕ and \mathbf{x} . The probability parameters γ and γ' can be

regarded as constants that can be chosen to be arbitrarily small. If $1/\cos \alpha$ grows slower than the square root of the width k , then the bound, up to a constant factor, is essentially $\sqrt{k/d} \rho \cos \alpha$.

Lemma 7. Suppose $\mathbf{x} \in \rho \mathbb{H}^d$ is such that $\phi^\top \mathbf{x} \neq 0$. Let $\alpha := \angle(\phi, \mathbf{x})$ and $y := \text{sgn}(\cos \alpha)$. Then with probability at least $1 - \gamma - \gamma'/\sqrt{2\pi}$ one has

$$y \sum_{j \in K^+} a_j \psi(\mathbf{w}_j^\top (\mathbf{p} + \mathbf{x})) > \frac{\sqrt{k} \rho}{\sqrt{d}} \left(\frac{\sqrt{\pi}}{4} |\cos \alpha| \left(\frac{1}{4\sqrt{2}} - \sqrt{\frac{\ln(1/\gamma)}{k}} \right) - \sqrt{\frac{2 \ln(1/\gamma')}{k}} \right),$$

provided that $\gamma' \leq 1/\sqrt{e}$.

Proof. Let us consider the case $y = 1$, i.e. $\phi^\top \mathbf{x} = \rho \cos \alpha > 0$.

We reason as follows, where $\stackrel{d}{=}$ denotes distributional equivalence:

$$\begin{aligned} & \sum_{j \in K^+} a_j \psi(\mathbf{w}_j^\top (\mathbf{p} + \mathbf{x})) \\ &= \sum_{j \in K^+} a_j \psi(\mathbf{w}_j^\top \mathbf{x}) && \text{since } j \in K^+ \text{ implies } \mathbf{w}_j^\top \mathbf{p} = 0 \\ &= \sum_{j \in K^+} \frac{\text{sgn}(\mathbf{w}_j^\top \phi)}{\sqrt{k}} \psi(\mathbf{w}_j^\top \mathbf{x}) && \text{by definition of } K^+ \\ &\stackrel{d}{=} \sum_{j \in [k]} B_j \frac{\text{sgn}(\mathbf{w}_j^\top \phi)}{\sqrt{k}} \psi(\mathbf{w}_j^\top \mathbf{x}) && \text{where } B_j \text{ are independent } \text{Ber}(1/2) \\ &= \sum_{\substack{B_j=1 \\ \mathbf{w}_j^\top \phi > 0 \\ \mathbf{w}_j^\top \mathbf{x} > 0}} \frac{\mathbf{w}_j^\top \mathbf{x}}{\sqrt{k}} - \sum_{\substack{B_{j'}=1 \\ \mathbf{w}_{j'}^\top \phi < 0 \\ \mathbf{w}_{j'}^\top \mathbf{x} > 0}} \frac{\mathbf{w}_{j'}^\top \mathbf{x}}{\sqrt{k}} && \text{by definition of } \psi \\ &= \sum_{\substack{B_j=1 \\ \mathbf{w}_j^\top \phi > 0 \\ \mathbf{w}_j^\top \mathbf{x} > 0}} \frac{\mathbf{w}_j^\top \mathbf{x}}{\sqrt{k}} + \sum_{\substack{B_{j'}=1 \\ -\mathbf{w}_{j'}^\top \phi > 0 \\ -\mathbf{w}_{j'}^\top \mathbf{x} < 0}} \left(-\frac{\mathbf{w}_{j'}^\top \mathbf{x}}{\sqrt{k}} \right) && \text{and observe } j \text{ and } j' \text{ are disjoint} \\ &\stackrel{d}{=} \sum_{\substack{B_j=1 \\ \mathbf{w}_j^\top \phi > 0 \\ \mathbf{w}_j^\top \mathbf{x} > 0}} \frac{\mathbf{w}_j^\top \mathbf{x}}{\sqrt{k}} + \sum_{\substack{B_{j'}=1 \\ \mathbf{w}_{j'}^\top \phi > 0 \\ \mathbf{w}_{j'}^\top \mathbf{x} < 0}} \frac{\mathbf{w}_{j'}^\top \mathbf{x}}{\sqrt{k}} && \text{by independence and symmetry of } \mathbf{w}_{j'} \\ &= \sum_{\substack{B_j=1 \\ \mathbf{w}_j^\top \phi > 0}} \frac{\mathbf{w}_j^\top \mathbf{x}}{\sqrt{k}} && \text{by merging the sums} \\ &= \sum_{\substack{B_j=1 \\ \mathbf{w}_j^\top \phi > 0}} \frac{\mathbf{w}_j^\top \phi \phi^\top \mathbf{x}}{\sqrt{k}} + \sum_{\substack{B_j=1 \\ \mathbf{w}_j^\top \phi > 0}} \frac{\mathbf{w}_j^\top (\mathbf{I}_d - \phi \phi^\top) \mathbf{x}}{\sqrt{k}} && \text{projecting onto } \phi \text{ and orthogonal hyperplane} \\ &\stackrel{d}{=} \underbrace{\sum_{B'_j=1} \frac{|\mathbf{w}_j^\top \phi| \phi^\top \mathbf{x}}{\sqrt{k}}}_{\text{(I)}} + \underbrace{\sum_{B'_j=1} \frac{\mathbf{w}_j^\top (\mathbf{I}_d - \phi \phi^\top) \mathbf{x}}{\sqrt{k}}}_{\text{(II)}} && \text{where } B'_j \text{ are independent } \text{Ber}(1/4). \end{aligned}$$

We now analyse the two sums separately, in both cases obtaining a lower bound:

- (I) Each of the k terms is the absolute value of an independent centred Gaussian with variance $(\rho \cos \alpha)^2/(dk)$, so it is with probability $1/2$ greater than

$$\frac{\sqrt{2} \operatorname{erf}^{-1}(1/2) \rho \cos \alpha}{\sqrt{dk}} > \frac{\sqrt{\pi} \rho \cos \alpha}{2\sqrt{2dk}}.$$

Also each of the k terms is present in the sum independently with probability $1/4$. Hence by Hoeffding's inequality (see e.g. Vershynin [2018, Theorem 2.2.6]), we have that with probability at least $1 - \gamma$ the sum is greater than

$$\frac{\sqrt{\pi} \rho \cos \alpha}{2\sqrt{2dk}} \left(\frac{k}{8} - \sqrt{\frac{k \ln(1/\gamma)}{2}} \right) = \frac{\sqrt{\pi k} \rho \cos \alpha}{4\sqrt{d}} \left(\frac{1}{4\sqrt{2}} - \sqrt{\frac{\ln(1/\gamma)}{k}} \right). \quad (2)$$

- (II) Each term is an independent centred Gaussian with variance $(\rho \sin \alpha)^2/(dk)$, so a sum of k' such terms is a centred Gaussian with variance $(\rho \sin \alpha)^2 k'/(dk)$, which is with probability at least $1 - \gamma'/\sqrt{2\pi}$ at least

$$-\rho |\sin \alpha| \sqrt{\frac{2k' \ln(1/\gamma')}{dk}} \geq -\rho \sqrt{\frac{2 \ln(1/\gamma')}{d}}, \quad \text{provided } \gamma' \leq 1/\sqrt{e}. \quad (3)$$

Summing the bounds in (2) and (3) yields the bound in the statement, and we can combine the probabilities by the union bound.

The case $y = -1$, i.e. $\phi^\top \mathbf{x} = \rho \cos \alpha < 0$, is analogous. \square

Second we prove a lemma that gives us a bound on how much the sum of outputs of the “unhelpful” neurons can spoil the work of the “helpful” neurons which the previous lemma addressed. The function f is the density of a standard Gaussian, i.e. $f(u) = e^{-u^2/2}/\sqrt{2\pi}$. It bounds the first summand inside the outer parentheses, which is therefore exponentially small for large $d/(\sqrt{k}\rho)$. Again viewing the probability parameter γ'' as arbitrarily small but constant, the second summand approaches zero at the rate of the square root of the width k . The techniques we use in the proof are similar to those in the previous one.

Lemma 8. *Suppose $\mathbf{x} \in \rho \mathbb{H}^d$ is such that $\phi^\top \mathbf{x} \neq 0$. Let $\alpha := \angle(\phi, \mathbf{x})$ and $y := \operatorname{sgn}(\cos \alpha)$. Then with probability at least $1 - \gamma''$ one has*

$$y \sum_{j \in K^-} a_j \psi(\mathbf{w}_j^\top (\mathbf{p} + \mathbf{x})) > -\frac{\sqrt{k}\rho}{\sqrt{d}} \left(f\left(\frac{d}{\sqrt{k}\rho}\right) \min\left\{1, \left(\frac{\sqrt{k}\rho}{d}\right)^2\right\} + \frac{2\pi}{\pi-1} \sqrt{\frac{\ln(1/\gamma'')}{k}} \right).$$

Proof. Let us consider the case $y = 1$, i.e. $\phi^\top \mathbf{x} = \rho \cos \alpha > 0$.

We estimate as follows:

$$\begin{aligned} & \sum_{j \in K^-} a_j \psi(\mathbf{w}_j^\top (\mathbf{p} + \mathbf{x})) \\ &= \sum_{j \in K^-} a_j \psi(\mathbf{w}_j^\top \mathbf{x} - \sqrt{d/|K^-|}) && \text{since } j \in K^- \text{ implies } \mathbf{w}_j^\top \mathbf{p} = -\sqrt{d/|K^-|} \\ &\geq - \sum_{j \in K^+} \frac{\psi(\mathbf{w}_j^\top \mathbf{x} - \sqrt{d/|K^-|})}{\sqrt{k}} && \text{since } a_j \geq -1/\sqrt{k} \\ &\geq - \sum_{j \in K^+} \frac{\psi(\mathbf{w}_j^\top \mathbf{x} - U)}{\sqrt{k}} && \text{where } U := \sqrt{d/k} \\ &\geq - \sum_{j \in [k]} \frac{\psi(\mathbf{w}_j^\top \mathbf{x} - U)}{\sqrt{k}} && \text{since } \psi(u) \geq 0 \text{ for all } u. \end{aligned}$$

Each $\mathbf{w}_j^\top \mathbf{x}$ is a centred Gaussian with variance $\rho^2/d =: \sigma^2$. Hence (see e.g. Vershynin [2018, Proposition 2.1.2])

$$\mathbb{P}\{\mathbf{w}_j^\top \mathbf{x} \geq U\} \geq \max\{\sigma/U - (\sigma/U)^3, 0\} \cdot f(U/\sigma).$$

We therefore have

$$\begin{aligned} \mu &:= \mathbb{E}[\psi(\mathbf{w}_j^\top \mathbf{x} - U)] = \int_U^\infty (u - U) \frac{f(u/\sigma)}{\sigma} du \\ &= \sigma f(U/\sigma) - U \mathbb{P}\{\mathbf{w}_j^\top \mathbf{x} \geq U\} \leq \sigma f(U/\sigma) \min\{1, (\sigma/U)^2\}. \end{aligned}$$

Writing X_j for the centred random variable $\psi(\mathbf{w}_j^\top \mathbf{x} - U) - \mu$, there are the following two cases.

Case $0 \leq s \leq \mu$.

$$\begin{aligned} \mathbb{P}\{|\mathbf{w}_j^\top \mathbf{x}| \geq s\} &\geq \mathbb{P}\{|\mathbf{w}_j^\top \mathbf{x}| \geq \mu\} = 1 - \int_{-\mu}^\mu \frac{f(u/\sigma)}{\sigma} du > 1 - 2\mu f(0)/\sigma \\ &\geq 1 - 2f(0)f(U/\sigma) > 1 - \frac{1}{\pi} \geq \left(1 - \frac{1}{\pi}\right) \mathbb{P}\{|X_j| \geq s\}. \end{aligned}$$

Case $\mu < s$.

$$\mathbb{P}\{|\mathbf{w}_j^\top \mathbf{x}| \geq s\} \geq 2\mathbb{P}\{\mathbf{w}_j^\top \mathbf{x} \geq U + \mu + s\} = 2\mathbb{P}\{\psi(\mathbf{w}_j^\top \mathbf{x} - U) \geq \mu + s\} = 2\mathbb{P}\{|X_j| \geq s\}.$$

Hence X_j is sub-Gaussian with parameter $\sqrt{2\pi}\sigma/(\pi-1)$ (see e.g. Wainwright [2019, proof of Theorem 2.6]), so by Hoeffding's bound (see e.g. Wainwright [2019, Proposition 2.5]), with probability at least $1 - \gamma''$ one has

$$\begin{aligned} \sum_{j \in K^-} a_j \psi(\mathbf{w}_j^\top (\mathbf{p} + \mathbf{x})) &\geq - \sum_{j \in [k]} \frac{\mu + X_j}{\sqrt{k}} = -\sqrt{k}\mu - \sum_{j \in [k]} \frac{X_j}{\sqrt{k}} \\ &> -\sqrt{k}\mu - \frac{2\pi}{\pi-1} \sigma \sqrt{\ln(1/\gamma'')} \geq -\sqrt{k} \sigma f(U/\sigma) \min\{1, (\sigma/U)^2\} - \frac{2\pi}{\pi-1} \sigma \sqrt{\ln(1/\gamma'')} \\ &= -\frac{\sqrt{k}\rho}{\sqrt{d}} f\left(\frac{d}{\sqrt{k}\rho}\right) \min\left\{1, \left(\frac{\sqrt{k}\rho}{d}\right)^2\right\} - \frac{2\pi}{\pi-1} \rho \sqrt{\frac{\ln(1/\gamma'')}{d}}, \end{aligned}$$

which equals the bound in the statement.

The case $y = -1$, i.e. $\phi^\top \mathbf{x} = \rho \cos \alpha < 0$, is again analogous. \square

We now restate and prove Theorem 1 from Section 2.

Theorem 1. *There exist constants C_1, C_2, C_3, C_4 and C_5 such that, with probability at least $(1 - C_1\gamma)(1 - \gamma^\dagger)$ over the choice of the network \mathcal{N} and the labelled data point (\mathbf{x}, y) sampled from the (ϕ, ρ, τ) -Bernoulli distribution, provided that $2d\tau^2 \geq \ln(1/\gamma^\dagger)$, we have*

$$y \mathcal{N}(\mathbf{p} + \mathbf{x}) > \frac{\sqrt{k}\rho}{\sqrt{d}} \left(C_2\tau - C_3 \exp\left(-\frac{d^2}{2k\rho^2}\right) \min\left\{1, \frac{k\rho^2}{d^2}\right\} - C_4 \sqrt{\frac{\ln(1/\gamma)}{k}} - C_5 \sqrt{\frac{\ln(1/\gamma^\dagger)}{d}} \right).$$

Proof. Let $\alpha := \angle(\phi, \mathbf{x})$.

Since (\mathbf{x}, y) is sampled from the (ϕ, ρ, τ) -Bernoulli distribution, Schmidt et al. [2018, Lemma 24] tell us that, for all $u \in (0, 2\tau]$,

$$\mathbb{P}\{y \cos \alpha > 2\tau - u\} \geq 1 - e^{-du^2/2},$$

i.e. that with probability at least $1 - \gamma^\dagger$ one has

$$y \cos \alpha > 2\tau - \sqrt{\frac{2 \ln(1/\gamma^\dagger)}{d}},$$

provided that $2d\tau^2 \geq \ln(1/\gamma^\dagger)$.

It remains to apply Lemmas 7 and 8 with $\gamma = \gamma' = \gamma''$ and $C_1 = 2 + 1/\sqrt{2\pi}$, observe that $1 - C_1\gamma \geq 0$ implies $\gamma \leq 1/\sqrt{e}$, and simplify as follows:

$$\begin{aligned} & \frac{\sqrt{\pi}}{4} y \cos \alpha \left(\frac{1}{4\sqrt{2}} - \sqrt{\frac{\ln(1/\gamma)}{k}} \right) - \sqrt{\frac{2 \ln(1/\gamma)}{k}} \\ & - f\left(\frac{d}{\sqrt{k}\rho}\right) \min\left\{1, \left(\frac{\sqrt{k}\rho}{d}\right)^2\right\} - \frac{2\pi}{\pi-1} \sqrt{\frac{\ln(1/\gamma)}{k}} \\ & \geq \frac{\sqrt{\pi}}{16\sqrt{2}} y \cos \alpha - f\left(\frac{d}{\sqrt{k}\rho}\right) \min\left\{1, \left(\frac{\sqrt{k}\rho}{d}\right)^2\right\} \\ & \quad - \left(\sqrt{2} + \frac{\sqrt{\pi}}{4} + \frac{2\pi}{\pi-1}\right) \sqrt{\frac{\ln(1/\gamma)}{k}} \\ & > \frac{\sqrt{\pi}}{8\sqrt{2}} \tau - f\left(\frac{d}{\sqrt{k}\rho}\right) \min\left\{1, \left(\frac{\sqrt{k}\rho}{d}\right)^2\right\} \\ & \quad - \left(\sqrt{2} + \frac{\sqrt{\pi}}{4} + \frac{2\pi}{\pi-1}\right) \sqrt{\frac{\ln(1/\gamma)}{k}} - \frac{\sqrt{\pi}}{16} \sqrt{\frac{\ln(1/\gamma^\dagger)}{d}}, \end{aligned}$$

which establishes the statement with

$$C_2 = \frac{\sqrt{\pi}}{8\sqrt{2}}, \quad C_3 = 1/\sqrt{2\pi}, \quad C_4 = \sqrt{2} + \frac{\sqrt{\pi}}{4} + \frac{2\pi}{\pi-1} \quad \text{and} \quad C_5 = \frac{\sqrt{\pi}}{16}. \quad \square$$

We also restate and prove Corollary 2 from Section 2.

Corollary 2. *Suppose that*

$$k = \Omega(d^{\eta(k)}), \quad \rho = O(d^{\eta(\rho)}), \quad 1/\tau = O(d^{\eta(\tau)}) \quad \text{and} \quad 1/\tau = \omega_d(1),$$

where $\eta(k), \eta(\rho), \eta(\tau) \in [0, 1]$ are arbitrary constants that satisfy

$$\eta(\rho) < 1 - \eta(k)/2 \quad \text{and} \quad \eta(\tau) < \eta(k)/2.$$

Then, for sufficiently large input dimensions d , the expected accuracy of the adversarially reprogrammed network \mathcal{N} on the (ϕ, ρ, τ) -Bernoulli data model is arbitrarily close to 100%.

Proof. Fix γ and γ^\dagger such that $(1 - C_1\gamma)(1 - \gamma^\dagger)$ is as close to 100% as required.

By the assumptions in the statement, and recalling that $k \leq d$, we have

$$\exp\left(\frac{d^2}{k\rho^2}\right) = \Omega((1/\tau)^2), \quad \frac{k}{\ln(1/\gamma)} = \omega((1/\tau)^2) \quad \text{and} \quad \frac{d}{\ln(1/\gamma^\dagger)} = \omega((1/\tau)^2).$$

In particular, we have $2d\tau^2 \geq \ln(1/\gamma^\dagger)$ for large enough d .

The corollary follows by applying Theorem 1 and observing that

$$\begin{aligned} C_2\tau - C_3 \exp\left(-\frac{d^2}{2k\rho^2}\right) \min\left\{1, \frac{k\rho^2}{d^2}\right\} - C_4\sqrt{\frac{\ln(1/\gamma)}{k}} - C_5\sqrt{\frac{\ln(1/\gamma^\dagger)}{d}} \\ \geq \frac{1}{O(1/\tau)} - \frac{1}{\Omega(1/\tau) \ln(\Omega((1/\tau)^2))} - \frac{1}{\omega(1/\tau)} > \frac{1}{O(1/\tau)} - \frac{1}{\omega(1/\tau)} > 0. \quad \square \end{aligned}$$

C Clarke subdifferential

By Rademacher’s theorem, every locally Lipschitz function $g : \mathbb{R}^m \rightarrow \mathbb{R}$ is differentiable almost everywhere. Its Clarke subdifferential [Clarke, 1975] ∂g at a point z is the convex closure of the set of all limits of gradients along sequences that converge to z :

$$\partial g(z) := \text{conv} \left\{ \lim_{i \rightarrow \infty} \nabla g(z_i) \mid g \text{ differentiable at all } z_i, \text{ and } \lim_{i \rightarrow \infty} z_i = z \right\},$$

which is nonempty and compact. If g is continuously differentiable at z , then $\partial g(z) = \{\nabla g(z)\}$.

For example, the Clarke subdifferential of the ReLU function is:

$$\partial \psi(u) = \begin{cases} \{0\} & \text{if } u < 0, \\ [0, 1] & \text{if } u = 0, \\ \{1\} & \text{if } u > 0. \end{cases}$$

For a fuller introduction to the Clarke subdifferential and its applications to gradient flow, and for further references to related literature, we refer the reader to e.g. Lyu and Li [2020, Section 3 and Appendix I].

D Karush-Kuhn-Tucker conditions

Following Dutta, Deb, Tulshyan, and Arora [2013, Section 2.2], supposing $g, h_1, \dots, h_n : \mathbb{R}^m \rightarrow \mathbb{R}$ are locally Lipschitz, we have that $z \in \mathbb{R}^m$ is a Karush-Kuhn-Tucker point of the single-objective constrained optimisation problem

$$\text{minimise } g(z) \quad \text{subject to } \forall i \in [n] : h_i(z) \leq 0$$

if and only if there exist Lagrange multipliers $\lambda_1, \dots, \lambda_n \geq 0$ such that:

$$\text{(feasibility)} \quad \forall i \in [n] : h_i(z) \leq 0,$$

$$\text{(equilibrium inclusion)} \quad \mathbf{0} \in \partial g(z) + \sum_{i=1}^n \lambda_i \partial h_i(z), \text{ and}$$

$$\text{(complementary slackness)} \quad \forall i \in [n] : \lambda_i h_i(z) = 0.$$

E Proofs for implicit bias

Here we work with the notations and assumptions from Section 3, so we have a trajectory $\boldsymbol{\theta}(t) : [0, \infty) \rightarrow \mathbb{R}^{k(d+1)}$ of gradient flow for a two-layer ReLU network \mathcal{N} with input dimension d and width k , trained on an orthogonally separable binary classification dataset $S = \{(\mathbf{x}_1, y_1), \dots, (\mathbf{x}_n, y_n)\}$, from a balanced and live initialisation, using either the exponential $\ell_{\text{exp}}(u) = e^{-u}$ or the logistic $\ell_{\text{log}}(u) = \ln(1 + e^{-u})$ loss function.

For $t \in [0, \infty)$, we denote by $\mathcal{N}_{\boldsymbol{\theta}(t)}$ the network at time t of gradient flow, i.e. whose weights are the coordinates of the trajectory vector at time t : $\mathbf{w}_1(t), \dots, \mathbf{w}_k(t)$ for the first layer, and $a_1(t), \dots, a_k(t)$ for the second layer.

Since our network functions, loss functions, and their compositions, are definable (see Davis, Drusvyatskiy, Kakade, and Lee [2020, Corollary 5.11]), they admit the chain rule (see Davis et al. [2020, Theorem 5.8]), and hence we have the following basic fact on the empirical loss $\mathcal{L}(\boldsymbol{\theta}) = \sum_{i=1}^n \ell(y_i \mathcal{N}_{\boldsymbol{\theta}}(\mathbf{x}_i))$ decreasing along gradient flow.

Proposition 9 (by Davis et al. [2020, Lemma 5.2]). *We have $d\mathcal{L}(\boldsymbol{\theta})/dt = -\|d\boldsymbol{\theta}/dt\|^2$ for almost all $t \in [0, \infty)$.*

From the differential inclusion of gradient flow, i.e. that $d\boldsymbol{\theta}/dt \in -\partial\mathcal{L}(\boldsymbol{\theta}(t))$ for almost all $t \in [0, \infty)$, it is straightforward to obtain the following expressions for the derivatives of the weights during training. Note that for the first-layer we have a membership rather than an equation because the Clarke subdifferentials of the ReLU function may be at zero.

Proposition 10. *For all $j \in [k]$ and almost all $t \in [0, \infty)$ we have*

$$\begin{aligned} \frac{d\mathbf{w}_j}{dt} &\in - \sum_{i=1}^n \ell'(y_i \mathcal{N}_{\boldsymbol{\theta}}(\mathbf{x}_i)) y_i a_j \partial\psi(\mathbf{w}_j^\top \mathbf{x}_i) \mathbf{x}_i \\ \frac{da_j}{dt} &= - \sum_{i=1}^n \ell'(y_i \mathcal{N}_{\boldsymbol{\theta}}(\mathbf{x}_i)) y_i \psi(\mathbf{w}_j^\top \mathbf{x}_i). \end{aligned}$$

We now extend to exponential loss the observation made for logistic loss by Phuong and Lampert [2021, Lemma A.4]: that during training second-layer weights remain balanced and keep their signs.

Lemma 11. *Throughout the training, for all $j \in [k]$, we have that $|a_j| = \|\mathbf{w}_j\|$ and that a_j maintains its sign.*

Proof. Observe that the ReLU function satisfies $\partial\psi(u)u = \{\psi(u)\}$ for all $u \in \mathbb{R}$. Observe also that $|\ell'(u)| \leq \ell(u)$ for all $u \in \mathbb{R}$, which for exponential loss is trivial, and for logistic loss follows from $e < (1 + 1/e^u)e^{u+1}$, i.e. $1 < \ell_{\log}(u)/|\ell'_{\log}(u)|$.

From Proposition 10 it follows that $d\|\mathbf{w}_j\|^2/dt = 2\mathbf{w}_j^\top(d\mathbf{w}_j/dt)$ and $da_j^2/dt = 2a_j(da_j/dt)$, and so $d\|\mathbf{w}_j\|^2/dt = da_j^2/dt$ almost everywhere during the training.

Hence, by our assumption of balanced initialisation, we have that $|a_j| = \|\mathbf{w}_j\|$ throughout the training. Then, by Proposition 9, for almost all $t \in [0, \infty)$ we have that $a_j(t) \neq 0$ implies

$$\left| \frac{d \ln a_j^2(t)}{dt} \right| \leq 2 \sum_{i=1}^n |\ell'(y_i \mathcal{N}_{\boldsymbol{\theta}(t)}(\mathbf{x}_i))| \|\mathbf{x}_i\| \leq 2\mathcal{L}(\boldsymbol{\theta}(t)) \max_{i=1}^n \|\mathbf{x}_i\| \leq 2\mathcal{L}(\boldsymbol{\theta}(0)) \max_{i=1}^n \|\mathbf{x}_i\|.$$

Therefore $\ln a_j^2$ is bounded below by a linear function of t , so a_j does not cross zero throughout the training. \square

We now observe several key properties that the weights have during the training in our setting. Namely: the offsets of the positive neurons remain in the cone spanned by the positive inputs and the opposites of the negative inputs, their inner products with all the latter vectors are nondecreasing, and their norms either remain bounded or tend to infinity; and the analogous holds for the negative neurons. For $\mathbf{u}_1, \dots, \mathbf{u}_m \in \mathbb{R}^l$, let $\text{cone}(\mathbf{u}_1, \dots, \mathbf{u}_m) := \{\sum_{i=1}^m b_i \mathbf{u}_i \mid b_1, \dots, b_m \in [0, \infty)\}$. Also let $\mathbf{X} := \{y_i \mathbf{x}_i \mid i \in [n]\}$.

Lemma 12. (i) *For all $j \in [k]$ and all $t \in [0, \infty)$, we have $\mathbf{w}_j(t) - \mathbf{w}_j(0) \in \text{cone}(\text{sgn}(a_j)\mathbf{X})$.*

(ii) *For all $i \in [n]$, all $j \in [k]$, and almost all $t \in [0, \infty)$, we have $d(\mathbf{w}_j^\top \text{sgn}(a_j) y_i \mathbf{x}_i)/dt \geq 0$.*

(iii) *For each $j \in [k]$, either $|a_j|$ is bounded, or $|a_j| \rightarrow \infty$ as $t \rightarrow \infty$.*

Proof. We have (i) by Proposition 10 and the negativity of the derivatives of both the exponential and the logistic loss functions.

For (ii), we have by Proposition 10 that

$$\frac{d(\mathbf{w}_j^\top \operatorname{sgn}(a_j) y_i \mathbf{x}_i)}{dt} \in - \sum_{i'=1}^n \ell'(y_{i'} \mathcal{N}_\theta(\mathbf{x}_{i'})) |a_j| \partial \psi(\mathbf{w}_j^\top \mathbf{x}_{i'}) y_i y_{i'} \mathbf{x}_i^\top \mathbf{x}_{i'},$$

which never contains negative values since the dataset is orthogonally separable.

By Lemma 11, it suffices to show (iii) for $\|\mathbf{w}_j\|$, and so letting $\widehat{\mathbf{w}}_j(t) := \mathbf{w}_j(t) - \mathbf{w}_j(0)$, it suffices to show (iii) for $\|\widehat{\mathbf{w}}_j\|$.

Suppose $\widehat{\mathbf{w}}_j^\top(t) \operatorname{sgn}(a_j(t)) y_i \mathbf{x}_i$ is bounded for all $i \in [n]$. By orthogonal separability of the dataset, every two vectors in $\operatorname{cone}(\operatorname{sgn}(a_j) \mathbf{X})$ have nonnegative inner product, and so by (i) we have that

$$\|\widehat{\mathbf{w}}_j(t)\| \leq \sum_{i \in [n]} \frac{\widehat{\mathbf{w}}_j^\top(t) \operatorname{sgn}(a_j(t)) y_i \mathbf{x}_i}{\|\mathbf{x}_i\|}.$$

Hence $\|\widehat{\mathbf{w}}_j(t)\|$ is also bounded.

Otherwise, by (ii), there exists $i \in [n]$ such that $\widehat{\mathbf{w}}_j^\top(t) \operatorname{sgn}(a_j(t)) y_i \mathbf{x}_i \rightarrow \infty$ as $t \rightarrow \infty$. By orthogonal separability of the dataset, every two vectors in $\operatorname{cone}(\operatorname{sgn}(a_j) \mathbf{X})$ have nonnegative inner product, and so by (i) we have that

$$\frac{\widehat{\mathbf{w}}_j^\top(t) \operatorname{sgn}(a_j(t)) y_i \mathbf{x}_i}{\|\mathbf{x}_i\|} \leq \|\widehat{\mathbf{w}}_j(t)\|.$$

Hence also $\|\widehat{\mathbf{w}}_j(t)\| \rightarrow \infty$ as $t \rightarrow \infty$. □

The following is our main lemma, whose statement is simple: for every input, there must be at least one ReLU whose output tends to infinity during the training. For its proof, recall from Section 3 the notation $I_s = \{i \in [n] \mid y_i = s\}$.

Lemma 13. *For all $i \in [n]$, there exists $j \in [k]$ such that $\mathbf{w}_j^\top \mathbf{x}_i \rightarrow \infty$ as $t \rightarrow \infty$.*

Proof. Consider the case $i \in I_1$.

Recalling that $\mathbf{w}_{j_1}^\top \mathbf{x}_{i_1}$ is positive at $t = 0$ by our assumption of live initialisation, and that it is nondecreasing during the training by Lemma 12 (ii), we have by Lemma 11 that a_{j_1} is bounded below by a positive constant. Since $d(\mathbf{w}_{j_1}^\top \mathbf{x}_{i_1})/dt \geq -\ell'(\mathcal{N}_\theta(\mathbf{x}_{i_1})) a_{j_1} \|\mathbf{x}_{i_1}\|^2$ for almost all $t \in [0, \infty)$, we have that either $\mathcal{N}_\theta(\mathbf{x}_{i_1})$ or $\mathbf{w}_{j_1}^\top \mathbf{x}_{i_1}$ is not bounded above. In either case, by Lemma 12 (iii), there exists $j \in [k]$ such that $a_j \rightarrow \infty$ as $t \rightarrow \infty$.

Suppose $-\mathbf{w}_j^\top \mathbf{x}_{i'}$ is unbounded for some $i' \in I_{-1}$. Recalling that, by Lemma 12 (i), $\mathbf{w}_j(t) - \mathbf{w}_j(0) \in \operatorname{cone}(\mathbf{X})$ for all $t \in [0, \infty)$, it follows from orthogonal separability of the dataset that $-\mathbf{w}_j^\top \mathbf{x}_{i'}$ is unbounded for all $i' \in I_{-1}$. Hence there exists $T \in [0, \infty)$ such that, for all $i' \in I_{-1}$ and $t \in [T, \infty)$, we have $\mathbf{w}_j^\top \mathbf{x}_{i'} < 0$. Then $\mathbf{w}_j(t) - \mathbf{w}_j(T) \in \operatorname{cone}\{\mathbf{x}_i \mid i \in I_1\}$ for all $t \in [T, \infty)$, so $\mathbf{w}_j^\top \mathbf{x}_{i'}$ is unbounded for some $i' \in I_1$.

Therefore $\mathbf{w}_j^\top \mathbf{x}_{i'}$ is unbounded for some $i' \in I_1$. Arguing as before, since $\mathbf{w}_j(t) - \mathbf{w}_j(0) \in \operatorname{cone}(\mathbf{X})$ for all $t \in [0, \infty)$, we have that $\mathbf{w}_j^\top \mathbf{x}_{i'}$ is unbounded for all $i' \in I_1$, in particular for $i' = i$ as required.

The proof for the case $i \in I_{-1}$ is analogous. □

That brings us to a position where we can restate and prove Theorem 3 from Section 3. Using Lemma 13, we show that, whereas the empirical loss is bounded below by zero, eventually its rate of decrease remains at least the sum of squares of derivatives of the loss function, which implies that the latter and hence also the empirical loss get arbitrarily small.

Theorem 3. *There exists a time t_0 such that $\mathcal{L}(\theta(t_0)) < \ell(0)$.*

Proof. By Lemma 13, for each $i \in [n]$, let $j(i) \in [k]$ be such that $\mathbf{w}_{j(i)}^\top \mathbf{x}_i \rightarrow \infty$ as $t \rightarrow \infty$. Then let $T \in [0, \infty)$ be such that, for all $i \in [n]$ and all $t \in [T, \infty)$, we have $|a_{j(i)}| \geq 1/\|\mathbf{x}_i\|$ and $\mathbf{w}_{j(i)}^\top \mathbf{x}_i > 0$.

Recalling Propositions 9 and 10, for almost all $t \in [T, \infty)$ we have

$$\begin{aligned}
\frac{d\mathcal{L}(\boldsymbol{\theta})}{dt} &= - \left\| \frac{d\boldsymbol{\theta}}{dt} \right\|^2 \leq - \sum_{j=1}^k \left\| \frac{d\mathbf{w}_j}{dt} \right\|^2 \\
&\in - \sum_{j=1}^k \left\| \sum_{i=1}^n \ell'(y_i \mathcal{N}_{\boldsymbol{\theta}}(\mathbf{x}_i)) y_i a_j \partial \psi(\mathbf{w}_j^\top \mathbf{x}_i) \mathbf{x}_i \right\|^2 \\
&\subseteq - \sum_{j=1}^k \left(\sum_{i=1}^n \ell'(y_i \mathcal{N}_{\boldsymbol{\theta}}(\mathbf{x}_i)) y_i a_j \partial \psi(\mathbf{w}_j^\top \mathbf{x}_i) \mathbf{x}_i \right)^\top \left(\sum_{i'=1}^n \ell'(y_{i'} \mathcal{N}_{\boldsymbol{\theta}}(\mathbf{x}_{i'})) y_{i'} a_j \partial \psi(\mathbf{w}_j^\top \mathbf{x}_{i'}) \mathbf{x}_{i'} \right) \\
&= - \sum_{j=1}^k \sum_{i=1}^n \sum_{i'=1}^n \ell'(y_i \mathcal{N}_{\boldsymbol{\theta}}(\mathbf{x}_i)) \ell'(y_{i'} \mathcal{N}_{\boldsymbol{\theta}}(\mathbf{x}_{i'})) a_j^2 \partial \psi(\mathbf{w}_j^\top \mathbf{x}_i) \partial \psi(\mathbf{w}_j^\top \mathbf{x}_{i'}) y_i y_{i'} \mathbf{x}_i^\top \mathbf{x}_{i'} \\
&\leq \left\{ - \min_{i=1}^n \sum_{j=1}^k (\ell'(y_i \mathcal{N}_{\boldsymbol{\theta}}(\mathbf{x}_i)) a_j \partial \psi(\mathbf{w}_j^\top \mathbf{x}_i) \|\mathbf{x}_i\|)^2 \right\} \\
&\leq \left\{ - \min_{i=1}^n \sum_{j=1}^k (\ell'(y_i \mathcal{N}_{\boldsymbol{\theta}}(\mathbf{x}_i)) a_{j(i)} \partial \psi(\mathbf{w}_{j(i)}^\top \mathbf{x}_i) \|\mathbf{x}_i\|)^2 \right\} \\
&\leq \left\{ - \sum_{i=1}^n (\ell'(y_i \mathcal{N}_{\boldsymbol{\theta}}(\mathbf{x}_i)))^2 \right\},
\end{aligned}$$

where the second inequality is by orthogonal separability of the dataset.

Hence $\mathcal{L}(\boldsymbol{\theta}(T)) \geq \int_T^\infty \sum_{i=1}^n (\ell'(y_i \mathcal{N}_{\boldsymbol{\theta}}(\mathbf{x}_i)))^2 dt$, so for all $\nu > 0$ there exists $t \in [T, \infty)$ such that $\sum_{i=1}^n (\ell'(y_i \mathcal{N}_{\boldsymbol{\theta}}(\mathbf{x}_i)))^2 < \nu$.

For exponential loss, let t_0 be such that $\sum_{i=1}^n (\ell'_{\exp}(y_i \mathcal{N}_{\boldsymbol{\theta}(t_0)}(\mathbf{x}_i)))^2 < 1/n^2$. Then for all $i \in [n]$ we have $y_i \mathcal{N}_{\boldsymbol{\theta}(t_0)}(\mathbf{x}_i) > \ln n$, so $\mathcal{L}(\boldsymbol{\theta}(t_0)) < 1 = \ell_{\exp}(0)$.

For logistic loss, let t_0 be such that $\sum_{i=1}^n (\ell'_{\log}(y_i \mathcal{N}_{\boldsymbol{\theta}(t_0)}(\mathbf{x}_i)))^2 < 1/(2n+1)^2$. Then for all $i \in [n]$ we have $y_i \mathcal{N}_{\boldsymbol{\theta}(t_0)}(\mathbf{x}_i) > \ln(2n)$ and thus $\ell_{\log}(y_i \mathcal{N}_{\boldsymbol{\theta}(t_0)}(\mathbf{x}_i)) < \ln(1 + 1/(2n)) < 1/(2n)$, so $\mathcal{L}(\boldsymbol{\theta}(t_0)) < 1/2 < \ln 2 = \ell_{\log}(0)$. \square

The following theorem from recent literature is on the late phase of gradient flow, i.e. after attaining perfect accuracy and a small loss. Its assumptions on the network are satisfied in our setting (see Ji and Telgarsky [2020, Section 2]), in particular two-layer ReLU networks are positively 2-homogeneous, i.e. for all $\alpha > 0$, $\boldsymbol{\theta}$ and \mathbf{x} , we have $\mathcal{N}_{\alpha\boldsymbol{\theta}}(\mathbf{x}) = \alpha^2 \mathcal{N}_{\boldsymbol{\theta}}(\mathbf{x})$. For KKT conditions for nonsmooth optimisation problems, see Appendix D.

Theorem 14 (Lyu and Li [2020, Theorem A.8] and Ji and Telgarsky [2020, Theorem 3.1]). *Suppose $\mathcal{N}_{\boldsymbol{\theta}}$ is a neural network which is locally Lipschitz, positively homogeneous, and definable in some o-minimal structure that includes the exponential function. Consider minimising either the exponential or the logistic loss over a binary classification dataset $(\mathbf{x}_1, y_1), \dots, (\mathbf{x}_n, y_n)$ using gradient flow. If $\mathcal{L}(\boldsymbol{\theta}(0)) < \ell(0)$, then as $t \rightarrow \infty$ we have that $\mathcal{L}(\boldsymbol{\theta}(t)) \rightarrow 0$, $\|\boldsymbol{\theta}(t)\| \rightarrow \infty$, and the weights converge in direction to a Karush–Kuhn–Tucker point of the following maximum margin problem:*

$$\text{minimise } \frac{1}{2} \|\boldsymbol{\theta}\|^2 \quad \text{subject to } \forall i \in [n] : y_i \mathcal{N}_{\boldsymbol{\theta}}(\mathbf{x}_i) \geq 1.$$

Another recent result is the next lemma, which shows that maximum-margin KKT points for two-layer ReLU networks on orthogonally separable datasets are particularly streamlined. Recall from

Section 3 that \mathbf{v}_1 and \mathbf{v}_{-1} denote the maximum margin vectors for the positive and negative data classes, respectively. We remark that it may be interesting that a part of the statement says that, regardless of whether the initialisation was balanced, the weights of any KKT point are balanced. We provide a proof of the lemma, which is perhaps simpler, and also it removes a marginal concern about applicability to our setting due to the leaky ReLU activation having been assumed in Lyu et al. [2021, Lemma B.9].

Lemma 15 (Lyu et al. [2021, Lemma H.3]). *Suppose $\boldsymbol{\theta}$ is a Karush–Kuhn–Tucker point of the problem in Theorem 14 for a two-layer ReLU network $\mathcal{N}_\boldsymbol{\theta}$ and an orthogonally separable dataset. Then for all $j \in [k]$ we have $|a_j| = \|\mathbf{w}_j\|$, and if $a_j \neq 0$ then*

$$\frac{\mathbf{w}_j}{\|\mathbf{w}_j\|} = \frac{\mathbf{v}_{\text{sgn}(a_j)}}{\sum_{\text{sgn}(a_{j'})=\text{sgn}(a_j)} a_{j'}^2}.$$

Proof. We have that $\boldsymbol{\theta}$ is feasible, i.e. $\forall i \in [n] : y_i \mathcal{N}_\boldsymbol{\theta}(\mathbf{x}_i) \geq 1$, and some $\lambda_1, \dots, \lambda_n \geq 0$ satisfy

$$\boldsymbol{\theta} \in \sum_{i=1}^n \lambda_i \partial(y_i \mathcal{N}_\boldsymbol{\theta}(\mathbf{x}_i)) \quad \text{and} \quad \forall i \in [n] : \lambda_i = 0 \vee y_i \mathcal{N}_\boldsymbol{\theta}(\mathbf{x}_i) = 1.$$

Thus, for all $j \in [k]$, we have $\mathbf{w}_j = a_j \sum_{i=1}^n \lambda_i y_i \psi'_{i,j} \mathbf{x}_i$ where $\psi'_{i,j} \in \partial \psi(\mathbf{w}_j^\top \mathbf{x}_i)$ are some values, and $a_j = \sum_{i=1}^n \lambda_i y_i \psi(\mathbf{w}_j^\top \mathbf{x}_i)$.

That $a_j = 0$ implies $\|\mathbf{w}_j\| = 0$ is immediate, so suppose $a_j > 0$.

For all $i' \in I_{-1}$ such that $\lambda_{i'} > 0$, we have by orthogonal separability that

$$\mathbf{w}_j^\top \mathbf{x}_{i'} = a_j \sum_{i=1}^n \lambda_i y_i \psi'_{i,j} \mathbf{x}_i^\top \mathbf{x}_{i'} \leq -a_j \lambda_{i'} \psi'_{i',j} \|\mathbf{x}_{i'}\|^2,$$

so $\psi'_{i',j} > 0$ is impossible, and thus $\psi'_{i',j} = 0$.

Hence $a_j = \sum_{i \in I_1} \lambda_i \psi(\mathbf{w}_j^\top \mathbf{x}_i)$, so there exists $i \in I_1$ such that $\lambda_i > 0$ and $\mathbf{w}_j^\top \mathbf{x}_i > 0$. Then for all $i' \in I_1$ we have $\mathbf{w}_j^\top \mathbf{x}_{i'} \geq a_j \lambda_i \mathbf{x}_i^\top \mathbf{x}_{i'} > 0$.

Therefore $a_j^2 = \mathbf{w}_j^\top a_j \sum_{i \in I_1} \lambda_i \mathbf{x}_i = \|\mathbf{w}_j\|^2$, so $a_j = \|\mathbf{w}_j\|$ and $\mathbf{w}_j / \|\mathbf{w}_j\| = \sum_{i \in I_1} \lambda_i \mathbf{x}_i =: \mathbf{u}_1$.

Analogously, if $a_j < 0$, then $-a_j = \|\mathbf{w}_j\|$ and $\mathbf{w}_j / \|\mathbf{w}_j\| = \sum_{i \in I_{-1}} \lambda_i \mathbf{x}_i =: \mathbf{u}_{-1}$.

For both signs $s \in \{\pm 1\}$, let $\kappa_s := \sum_{\text{sgn}(a_j)=s} a_j^2$. By orthogonal separability, it follows that for all $i \in I_s$ we have $\mathcal{N}_\boldsymbol{\theta}(\mathbf{x}_i) = \sum_{\text{sgn}(a_j)=s} a_j \mathbf{w}_j^\top \mathbf{x}_i = \kappa_s \mathbf{u}_s^\top \mathbf{x}_i$. Hence $\kappa_s \mathbf{u}_s$ is a Karush-Kuhn-Tucker point of the maximum margin problem

$$\text{minimise } \frac{1}{2} \|\mathbf{v}\|^2 \quad \text{subject to } \forall i \in I_s : \mathbf{v}^\top \mathbf{x}_i \geq 1,$$

and therefore its unique Karush-Kuhn-Tucker point, which is the maximum margin vector \mathbf{v}_s . \square

The following corollary, restated from Section 3, is now an immediate consequence of Theorem 3, Theorem 14 and Lemma 15.

Corollary 4. *As the time tends to infinity, we have that the empirical loss converges to zero, the Euclidean norm of the weights converges to infinity, and the weights converge in direction to some $\boldsymbol{\theta}$ such that for all $j \in [k]$ we have $|a_j| = \|\mathbf{w}_j\|$, and if $a_j \neq 0$ then*

$$\frac{\mathbf{w}_j}{\|\mathbf{w}_j\|} = \frac{\mathbf{v}_{\text{sgn}(a_j)}}{\sum_{\text{sgn}(a_{j'})=\text{sgn}(a_j)} a_{j'}^2}.$$

It remains to prove Proposition 5, also restated from Section 3.

Proposition 5. Suppose weights θ are as in Corollary 4, class label mapping $m \in \{\pm 1\}$ is arbitrary, data model \mathcal{D} is any (ϕ, ρ, τ) -Bernoulli distribution such that $m \cos \angle(\mathbf{v}_1 - \mathbf{v}_{-1}, \phi) < 0$, and adversarial program \mathbf{p} is arbitrary. Then we have that

$$\mathbb{P}_{(\mathbf{x}, y) \sim \mathcal{D}}\{m y \mathcal{N}_{\theta}(\mathbf{p} + \mathbf{x}) > 0\} \leq \frac{1}{2} + \frac{1}{2} e^{-2d\tau^2 \cos^2 \angle(\mathbf{v}_1 - \mathbf{v}_{-1}, \phi)}.$$

Proof. The cases $m = 1$ and $m = -1$ are symmetric by swapping ϕ and y with $-\phi$ and $-y$, so we can assume that $m = 1$.

Since

$$\begin{aligned} & \mathbb{P}_{(\mathbf{x}, y) \sim \mathcal{D}}\{y \mathcal{N}_{\theta}(\mathbf{p} + \mathbf{x}) > 0\} \\ &= \frac{1}{2} \mathbb{P}_{(\mathbf{x}, y) \sim \mathcal{D}}\{y \mathcal{N}_{\theta}(\mathbf{p} + \mathbf{x}) > 0 \mid y = 1\} + \frac{1}{2} \mathbb{P}_{(\mathbf{x}, y) \sim \mathcal{D}}\{y \mathcal{N}_{\theta}(\mathbf{p} + \mathbf{x}) > 0 \mid y = -1\}, \end{aligned}$$

it suffices to establish the following claim: there exists a data class $s \in \{\pm 1\}$ such that

$$\mathbb{P}_{(\mathbf{x}, y) \sim \mathcal{D}}\{y \mathcal{N}_{\theta}(\mathbf{p} + \mathbf{x}) > 0 \mid y = s\} \leq e^{-2d\tau^2 \cos^2 \angle(\mathbf{v}_1 - \mathbf{v}_{-1}, \phi)}.$$

Suppose $\mathbf{v}_1^\top \mathbf{p} \leq \mathbf{v}_{-1}^\top \mathbf{p}$, and let $s = 1$. Then we have that $\psi(\mathbf{v}_1^\top(\mathbf{p} + \mathbf{x})) > \psi(\mathbf{v}_{-1}^\top(\mathbf{p} + \mathbf{x}))$ implies $\mathbf{v}_1^\top \mathbf{x} > \mathbf{v}_{-1}^\top \mathbf{x}$, so

$$\begin{aligned} & \mathbb{P}_{(\mathbf{x}, y) \sim \mathcal{D}}\{y \mathcal{N}_{\theta}(\mathbf{p} + \mathbf{x}) > 0 \mid y = s\} = \mathbb{P}_{(\mathbf{x}, 1) \sim \mathcal{D}}\{\mathcal{N}_{\theta}(\mathbf{p} + \mathbf{x}) > 0\} \\ &= \mathbb{P}_{(\mathbf{x}, 1) \sim \mathcal{D}}\{\psi(\mathbf{v}_1^\top(\mathbf{p} + \mathbf{x})) > \psi(\mathbf{v}_{-1}^\top(\mathbf{p} + \mathbf{x}))\} \leq \mathbb{P}_{(\mathbf{x}, 1) \sim \mathcal{D}}\{\mathbf{v}_1^\top \mathbf{x} > \mathbf{v}_{-1}^\top \mathbf{x}\} \\ &\leq e^{-2d\tau^2 \cos^2 \angle(\mathbf{v}_1 - \mathbf{v}_{-1}, \phi)} \end{aligned}$$

as required, where the last inequality is by the assumption $\cos \angle(\mathbf{v}_1 - \mathbf{v}_{-1}, \phi) < 0$ and Schmidt et al. [2018, Lemma 26].

If $\mathbf{v}_1^\top \mathbf{p} \geq \mathbf{v}_{-1}^\top \mathbf{p}$, the argument to show the claim is analogous, with taking $s = -1$ and observing that $\psi(\mathbf{v}_1^\top(\mathbf{p} + \mathbf{x})) < \psi(\mathbf{v}_{-1}^\top(\mathbf{p} + \mathbf{x}))$ implies $\mathbf{v}_1^\top \mathbf{x} < \mathbf{v}_{-1}^\top \mathbf{x}$. \square

F Data from experiments

Please see Tables 1 and 2.

Table 1: Data for the plots in Figure 3 on the left

	EfficientNet-B0	Inception-v3	ResNet-101V2	ResNet-152V2	ResNet-50	ResNet-50V2
$r = 2^{-5}$	81.5 %	80.4 %	68.3 %	54.1 %	73.1 %	61.2 %
$r = 2^{-\frac{40}{9}}$	87.2 %	85.7 %	59.8 %	50.3 %	82.1 %	66.7 %
$r = 2^{-\frac{35}{9}}$	89.4 %	85.0 %	75.9 %	57.3 %	80.9 %	72.3 %
$r = 2^{-\frac{30}{9}}$	91.8 %	88.8 %	70.3 %	33.5 %	83.4 %	81.4 %
$r = 2^{-\frac{25}{9}}$	87.5 %	80.1 %	77.8 %	52.1 %	83.7 %	77.1 %
$r = 2^{-\frac{20}{9}}$	85.6 %	84.2 %	64.7 %	32.6 %	75.4 %	69.3 %
$r = 2^{-\frac{15}{9}}$	86.8 %	10.7 %	68.2 %	39.8 %	52.2 %	55.4 %
$r = 2^{-\frac{10}{9}}$	17.4 %	18.0 %	70.5 %	45.0 %	4.6 %	66.8 %
$r = 2^{-\frac{5}{9}}$	68.5 %	0.0 %	29.1 %	27.6 %	0.0 %	51.9 %

Table 2: Data for the plots in Figure 3 on the right

	EfficientNet-B0	Inception-v3	ResNet-101V2	ResNet-152V2	ResNet-50	ResNet-50V2
$v = 2^{-10}$	13.0 %	11.6 %	10.5 %	9.6 %	10.2 %	10.1 %
$v = 2^{-\frac{80}{9}}$	61.1 %	54.9 %	67.7 %	10.8 %	72.5 %	61.4 %
$v = 2^{-\frac{70}{9}}$	80.9 %	84.8 %	83.7 %	64.0 %	88.1 %	75.3 %
$v = 2^{-\frac{60}{9}}$	85.6 %	82.8 %	81.6 %	81.4 %	89.6 %	78.4 %
$v = 2^{-\frac{50}{9}}$	92.3 %	88.7 %	88.9 %	86.7 %	90.5 %	82.5 %
$v = 2^{-\frac{40}{9}}$	93.7 %	91.4 %	90.2 %	85.4 %	92.8 %	89.5 %
$v = 2^{-\frac{30}{9}}$	94.6 %	90.2 %	75.2 %	69.7 %	87.9 %	80.1 %
$v = 2^{-\frac{20}{9}}$	95.1 %	88.5 %	56.4 %	26.9 %	83.9 %	76.6 %
$v = 2^{-\frac{10}{9}}$	93.4 %	65.8 %	29.7 %	21.2 %	51.0 %	51.0 %